Title of your paper: *Assessing the Impact of Wind Erosion in Baringo County, Kenya*

Author name: Cyrus Kimutai Kiprono

Affiliation: Jomo Kenyatta University of Agriculture and Technology (JKUAT)

Email: cyruskimutai40@gmail.com

ORCID link: https://orcid.org/my-orcid?orcid=0009-0009-7524-883X

Preprint statement:

This manuscript is a **non-peer-reviewed preprint** submitted to **EarthArXiv**.
The work is based on undergraduate research conducted for the award of a Bachelor of Science degree.
The manuscript has **not been submitted to a peer-reviewed journal**.

ASSESING IMPACT OF WIND EROSION ON SOIL LOSS A CASE STUDY OF BARINGO COUNTY.

by

CYRUS KIMUTAI KIPRONO

Department of Geomatic Engineering and Geospatial Information Systems (GEGIS)

ACKNOWLEDGEMENTS

I express my profound gratitude to the Almighty God for bestowing upon me good health all through my study period from beginning to completion. The unwavering strength, and a keen understanding, which were instrumental throughout the course of study and the completion of this project. The blessings of well-being provided a solid foundation for my academic pursuits.

I reserved special acknowledgment for Dr. Mercy Mwaniki, my esteemed supervisor, whose exceptional guidance, valuable advice, and unwavering support were invaluable assets to the successful completion of this project. Dr. Mwaniki's commitment, the time invested, and scholarly insights, along with her constructive criticism, greatly enhanced the quality and depth of my work. Her mentorship has been an indispensable aspect of my academic journey.

I extend heartfelt thanks to my family, particularly my parents, for their unwavering motivation, encouragement and above all their constant prayers. Their strong belief in my abilities has been a constant source of inspiration, fueling my determination to navigate the challenges in my studies and to always strive to do more in each step pertaining academics.

I also extend gratitude to the entire community of Geomatic Engineering and Geospatial Information Systems, encompassing both teaching and non-teaching staff. Their collective efforts have not only imparted knowledge but have also fostered an environment conducive to intellectual growth. I am forever indebted to this community for the wealth of insights and skills that will undoubtedly shape my future endeavors.

Table of Contents

LIST OF FIGURES

LIST OF TABLES

ACRONYMS AND ABBREVIATIONS

AE	Angstrom Exponent
CE	Climatic Erosivity
EF	Erodibility Fraction
FVRF	Friction Velocity Reduction Factor
GIS	Geographic Information System
ISRIC	World Soil Information
LULC	Land Use and Land Cover Changes
OBIA	Object-Based Image Analysis
OP	Optical Porosity
PCA1	First Principal Component
Qmax	Maximum Transport Capacity
RWEQ	Revised Wind Erosion Equation
SC	Soil Crust
SeaWiFS	Sea-viewing Wide Field-of-view Sensor
SR	Surface Roughness
USGS	United States Geological Survey
VC	Vegetation Cover
WEQ	Wind Erosion Equation
NASA	National Aeronautics and Space Administration
TM	Thematic Mapper
NIR	Near-Infrared
SWIR	Short-Wave Infrared
MODIS	Moderate Resolution Imaging Spectroradiometer

ABSTRACT

Wind erosion poses substantial threats to soil health and agricultural productivity in arid and semi-arid environments globally. In response to the escalating environmental challenge of wind erosion, this study, centered in Baringo County, employs a blend of remote sensing and GIS techniques alongside the Revised Wind Erosion Equation (RWEQ) model. The study spans a 25-year period, with a main objective of assessing the spatial-temporal impact of wind erosion on soil loss hence offering a long-term perspective on the dynamics of wind erosion.

The issue of soil destabilization and reduced agricultural productivity, primarily aggravated by land use changes and deforestation serves to fuel this study. These transformations prompt an urgent need for a comprehensive understanding of erosion processes and effective mitigation strategies. The methodology encompasses the utilization of Landsat data, Terra Climate data, and Africa Soil Grids data, to compute the parameters which serve as inputs for calculating Soil loss and mapping susceptibility by utilizing the RWEQ model.

The study demonstrates a steady rise in soil loss in Baringo County, increasing from 27.90 in 1995 to 35.96 Kg/Ha in 2020. Notably, 2005 marked a peak at 37.73 Kg/Ha. The study also evaluates the efficiency windbreaks in countering wind-induced soil erosion. Through analyses of average windbreak parameters such as width and optical porosity, the research provides quantitative insights into the effectiveness of these measures. The observed reduction in soil loss in Perkerra region in Baringo county from a maximum of 1.9 in 2010 to 0.8 kg/ha in 2020 supports the practical efficiency of windbreaks in mitigating erosive impacts, emphasizing their role as valuable tools in soil conservation strategies.

Keywords: Wind Erosion; Soil Loss; GIS; RWEQ.

CHAPTER 1: INTRODUCTION

This chapter focuses into the issue of wind erosion in Baringo County, Kenya. Section 1.1 begins by exploring what wind erosion entails in this region. The report captures how wind erosion, particularly in areas with minimal vegetation, significantly impacts the soil. Progressing further to section 1.2, the focus shifts to the critical reasons behind conducting this study in Baringo County. Motivated by the challenges posed by wind erosion to the landscape and its consequences for both the environment and communities, the study aims to bridge existing knowledge gaps.

The justification, captured in section 1.3 emphasizes the urgency of addressing erosion scars and the looming threat of desertification in Baringo County. The report highlights the study's commitment to unraveling the complexities of wind erosion's footprint in the region. Lastly, the goals of the research are outlined in section 1.4, outlining the objectives and research questions that underscore the importance of understanding the dynamics of human activities and natural forces in the context of wind erosion in Baringo County.

1.1 Background

Wind erosion is a natural process that occurs under dry conditions when bare soil with minimum vegetation cover is carried and transported by wind. Wind erosion is one of the key components of the complex land degradation process that threatens agricultural production and leads to hazardous landscapes. It is a serious environmental threat to which less attention has been given and has often been overlooked as a land degradation process until recently (Borrelli et al., 2017a).

Regions where minimal vegetation cover covers the land, wind erosion emerges as a profound ecological force, reshaping terrains with far-reaching consequences. The arid and semi-arid zones, comprising nearly one-third of the Earth's land surface, are particularly susceptible to wind erosion's impacts. Wind erosion stands as a vital environmental concern, extending across arid landscapes worldwide. Its impact is felt through the delicate balance of land degradation, triggering the loss of vital topsoil, essential nutrients, and ultimately jeopardizing the very bedrock of agricultural productivity.

Beyond its role in nutrient depletion, wind erosion plays a dual role, impacting both the land and the air. The winds that carry away soil particles hold within them the power to stir up dust storms, eroding not just the land's surface but also human well-being through compromised air quality, transportation hazards, and health risks. Among the many ways the land gets damaged, wind erosion stands out because of its many effects. It doesn't just make soil disappear, but it also starts a chain reaction that affects nature, money, and people's lives.

This chain reaction goes beyond hurting farms, it makes the air dirty, harms water sources, and causes sandstorms. Even though wind erosion has big effects like these, it hasn't been studied as much as other types of erosion like water erosion. This has led to a lack of research and understanding about it (Borrelli et al., 2017). However, considerable strides have been made in understanding the spatio-temporal dynamics and magnitudes of wind erosion.

These endeavors encompass both local and regional scales, utilizing a number of process-based and empirical models with varying degrees of complexity and applicability. A good example is the application of models that amalgamate key factors influencing wind erosion: climatic erosivity, soil erodibility, vegetation cover, and landscape roughness to delineate regions susceptible to this geomorphic process. (Borrelli et al., 2016; Saadoud et al., 2018; Fenta et al., 2020).

The investigation of wind erosion has undergone significant evolution, with notable contributions spanning several decades. In the 20th century, in 1990, Skidmore and Tatarko advanced the field by introducing stochastic wind simulation for erosion modeling, a pioneering approach that contributed to the understanding of wind erosion processes (Skidmore & Tatarko, 1990).

The 1990s to early 2000 witnessed a notable transition towards more sophisticated modeling techniques, as exemplified by the work of Zobeck et al. (2000). This study focused on scaling up wind erosion predictions from the field to regional scales, utilizing GIS and field-scale wind erosion models (Zobeck et al., 2000). This pivotal work laid the groundwork for future research, fostering a shift towards comprehensive regional assessments and influencing subsequent research methodologies in the field of wind erosion modeling.

Progressing into the 21st century, research on wind erosion expanded its horizons, incorporating advanced technologies like remote sensing and GIS. Borrelli et al. conducted a groundbreaking study providing a new assessment of soil loss due to wind erosion in European agricultural soils. The study employed a quantitative spatially distributed modeling approach, by utilizing the Revised Wind Erosion Equation offering a comprehensive and detailed understanding of the dynamics of wind erosion in the region (Borrelli et al., 2017a). This work significantly contributed to the refinement of modeling techniques, emphasizing the importance of spatial distribution in assessing soil loss due to wind erosion.

Subsequently, Chi et al. (2022a) explored the effects of land use/cover change on soil wind erosion in the Yellow River Basin since the 1990s, indicating a contemporary focus on understanding how human-induced changes impact wind erosion susceptibility (Chi et al., 2022a). The trends observed underline a progression from foundational observational studies to sophisticated modeling techniques and technology-driven assessments, emphasizing the dynamic nature of wind erosion research.

Through measurement, it is possible to test the efficacy of the intervention measures to combat wind erosion consequently ensuring that efforts to mitigate wind erosion yield meaningful results (Jarrah et al., 2020a). This highlights the pressing need to comprehensively address erosion concerns and foster sustainable land management practices to protect the regions affected by wind erosion.

Baringo County is a region defined by its arid landscape and expansive lowland grassland. Notably, this area has garnered attention as an erosion-prone zone, demonstrating the challenges posed by land degradation. The complex interaction between human activity, pastoralist land management practices, and land ownership has contributed to the portrayal of Baringo County as a desert-like environment (Boitt et al., 2020). In this context, the persistent wind erosion and its impact on soil quality pose significant concerns for the agricultural lands in the region, necessitating comprehensive mitigation strategies (Kangogo, 2021).

1.2 Motivation and Problem statement

Wind erosion stands as a critical environmental challenge in Baringo County, Kenya, with far-reaching consequences for both the natural ecosystem and human activities. The motivation behind this study arises from the urgent need to comprehend the intricate dynamics of wind erosion, considering its potential impact on soil composition and vegetative cover. Unlike water erosion, wind erosion's effects are often overlooked, and the limited research in this area has led to a gap in understanding.

Baringo County has a distinct landscape characterized by lowland grasslands and unique climatic patterns. Human-induced modifications through changes in land use practices and anthropogenic interventions have set in motion shifts in the delicate environmental equilibrium. The research aims to measure and quantify the induced soil loss by wind erosion, shedding light on the mechanics and consequences of this process.

The interplay between human actions and the erosive force of the wind constitutes a secondary catalyst for this investigation. As wind traverses the landscape, it seizes and transports soil particles, stripping away valuable topsoil. The goal is to unravel the interconnection between alterations in land use/cover and the amplification of soil wind erosion, striving to discern how human-induced modifications exacerbate this erosive process.

Mitigating wind erosion poses a significant challenge, particularly in assessing the efficiency of windbreaks due to limited field experiments. To overcome this challenge, the study proposes leveraging advanced technologies such as remote sensing and Geographic Information Systems (GIS) methodologies. This approach will provide an encompassing appraisal of windbreak performance and offer valuable insights into effective mitigation strategies.

1.3 Research identification and Objectives

The main objective of this project is to assess the spatial-temporal impact of wind erosion on soil loss in Baringo County, Kenya, covering the years 1995, 2000, 2005, 2010, 2015, and 2020. This is achievable through the following specific objectives:

I. To estimate the amount of soil lost as a result of wind erosion and analyze susceptibility of land to wind erosion.

II. To analyze the Impacts of land use land cover changes on soil wind erosion.

III. To evaluate the efficiency of windbreaks in protection against wind erosion using GIS and Remote sensing.

1.3.1 Research questions

The following questions are formulated with respect to aforementioned objectives:

I. How much soil is lost due to wind erosion annually, and what areas are most susceptible to wind erosion in the selected region?

II. How have land use and land cover changes over the past decade influenced the rates of soil loss due to wind erosion in the study area?

III. How effective are windbreaks in reducing wind erosion, and what is their impact on soil conservation as observed through GIS and remote sensing techniques?

1.4 Justification and Significance

The escalating threat of wind erosion and land degradation in Baringo County, Kenya, demands immediate attention due to its profound implications for the region's environmental sustainability. The intricate interplay of human activities and natural terrain characteristics has disrupted the delicate equilibrium of soil structure and vegetation cover. This poses a risk to soil fertility, agricultural productivity, and local ecosystems, threatening the livelihoods of the communities in Baringo County.

The visible erosion scars and the looming specter of desertification underscore the urgency of addressing the impact of wind erosion comprehensively. The significance of this study lies in its commitment to unraveling the dynamics of wind erosion's footprint in Baringo County. Through a combination of remote sensing, Geographic Information Systems (GIS), and empirical observations, the research aims to provide an understanding of the extent and patterns of wind erosion. The study thus seeks to guide effective interventions for sustainable land management and inform decision-making processes aimed at mitigating the adverse effects of wind erosion.

The provided images in Figure 1.1 and Figure 1.2 serve as visual evidence, depicting areas within Baringo County that have undergone significant degradation due to erosion. These images not only highlight the immediate and visible damage but also underscore the far-reaching consequences, including impacts on soil fertility, water quality, and the overall health of the ecosystem. By delving into the intricacies of wind erosion, this study aims to contribute valuable insights for the development of targeted conservation strategies, fostering sustainable land management practices and preserving the ecological integrity of Baringo County.

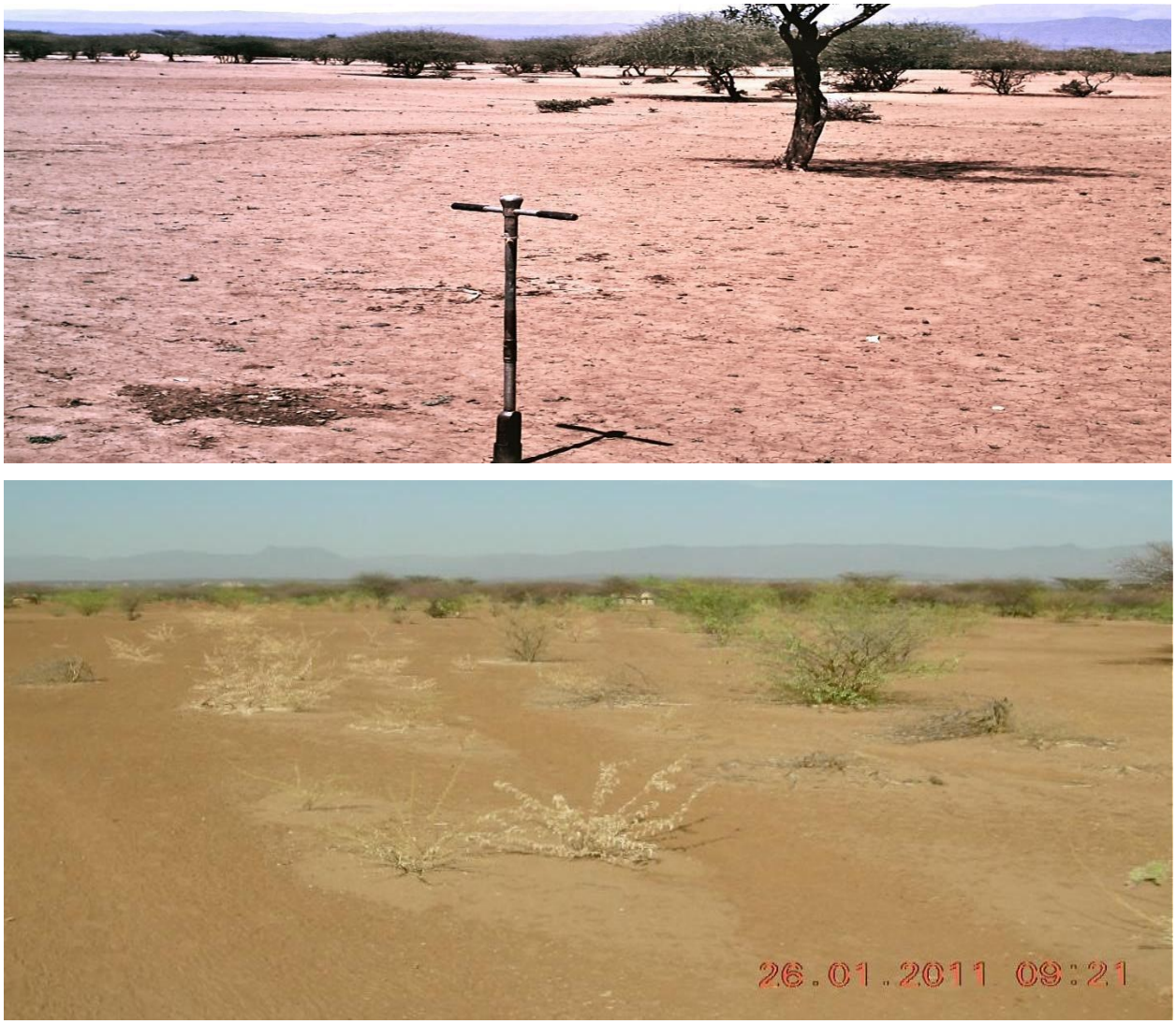

Figure 1.1(a): *Photo taken at Lamalok, Lake Baringo Basin. Severely degraded area (Aug. 2005),* ***(b)*** Open degraded communal rangelands *(Photos by Stephen*

1.5 Study outline

In Chapter 1, the study begins by addressing the serious issue of wind erosion in Baringo County, outlining the study's goals to assess soil loss, the impact of land use changes, and the effectiveness of windbreaks against erosion. This introductory chapter lays the groundwork for understanding the study's significance, the research questions it aims to answer, and its broader environmental implications. Following this, Chapter 2 delves into a comprehensive literature review, exploring existing studies on wind erosion, its mechanisms, influencing factors, and mitigation measures, particularly focusing on windbreaks. This review critically examines the gaps in current knowledge, setting a solid foundation for the study's methodology and analysis.

Chapters 3 through 5 take a more practical turn, with Chapter 3 detailing the methods used in the research, including data collection and analysis procedures. This chapter explains how the study quantifies soil loss, evaluates land use impacts, and assesses windbreak efficiency using GIS and remote sensing technologies. In Chapter 4, the study's findings are presented, analyzing the spatial-temporal patterns of wind erosion in Baringo County, the effects of land use and cover changes on soil erosion, and the success of windbreaks as a soil conservation strategy. Finally, Chapter 5 concludes the study by summarizing the findings, offering conclusions based on the research, and suggesting recommendations for future actions and studies.

CHAPTER 2: LITERATURE REVIEW

This chapter thoroughly looks into what others have found about wind erosion. In Section 2.1, it talks about the history of understanding wind erosion. Section 2.2 explores different ideas and models about how wind erosion happens. Section 2.3 reviews studies done in similar areas, explaining how they did their research and what they discovered. Section 2.4 looks at how wind erosion affects the environment, including soil, plants, and animals. Finally, in Section 2.5, it brings together all this information, points out what is still unknown, and explains how the research will add new knowledge.

2.1 Wind erosion processes and mechanism

The process of wind erosion as depicted in Figure 2.1 is a dynamic interplay of natural forces that results in the movement of sediment under the influence of wind. It can be broken down into three distinct phases i.e., deflation, transport and deposition (W. Cornelis, 2006). Deflation is the initial phase and it involves the removal of soil and sand particles from the surface due to the shear forces exerted by the wind. As the wind sweeps across the land, it picks up loose particles, initiating the process of erosion.

Once detached, these particles can be transported by the wind through various mechanisms, including creep, saltation, or suspension. The final phase involves the *deposition* of these transported particles. They can settle back to the ground through dry or wet removal processes.

Geospatial techniques, including GIS and remote sensing, play an important role in each phase of wind erosion analysis. In the deflation phase, high-resolution imagery helps identify and quantify soil and sand removal, pinpointing vulnerable areas affected by wind shear forces. For the transport phase, geospatial techniques track the movement of eroded particles, unravelling mechanisms like saltation and suspension. Finally, in the deposition phase, geospatial tools contribute to mapping the spatial distribution of deposited particles, offering insights into areas where sediment settles back to the ground.

Additionally, wind erosion can also involve a process known as abrasion. This is characterized by the sandblasting of rocks, soil aggregates, and crops by a stream of air laden with sediment. The mode of aeolian (wind-driven) sediment transport depends on both particle size and atmospheric flow conditions. Sand-sized particles, falling within the range of approximately 60-1000 μm, move primarily through saltation.

Very small dust-sized particles, smaller than 60 μm, are transported in suspension. They can remain airborne for extended periods and travel relatively long distances, dispersed beyond the atmospheric surface layer. Particles larger than 500 μm or less exposed particles can be pushed or rolled along the surface by the impact of saltating particles. This is referred to as surface creep.

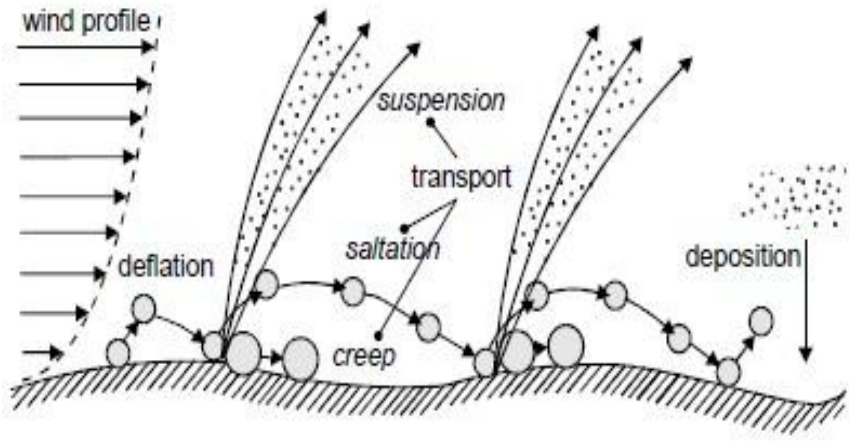

***Figure 2.1**:* Wind erosion Processes

2.2 Factors that influence wind erosion

Wind erosion is a complex process driven by a multitude of interacting factors that can be grouped into four distinct categories: *Meteorological Conditions, Soil Properties, Land-Surface Properties, Land-Use Practices*. Meteorological Conditions include crucial elements such as wind shear, precipitation, evaporation, humidity, and temperature. The erosivity of the wind is quantified by the shear velocity (u*), which measures the shear stress exerted by the wind. Precipitation and evaporation affect soil-water status, thus also influencing erodibility.

The erodibility of soil is expressed in terms of the threshold shear velocity (u*t), representing the minimal shear velocity required to initiate particle deflation. Particle size distribution, aggregate size distribution, and near-surface water status primarily determine u*t. Dynamic changes in soil properties necessitate u*t to be viewed as a time-variant parameter.

Soil-surface roughness, vegetation, and non-erodible elements forming Land-Surface Properties, significantly influence wind erosion processes. They impact both the magnitude of wind shear and the trapping of transported material. Soil-surface roughness, represented by microrelief, encompasses features like tillage ridges and clods. Vegetation, whether standing or flat, has been correlated with threshold shear velocity and trapping flux. Crusts formed through raindrop impact or cyanobacterial lichens protect against wind erosion, while field length determines mass transport rates across a field.

The various Land-Use Practices employed in land use have a profound impact on the other three categories. Properly implemented, they can acutely serve as effective wind-erosion control measures. These practices influence factors such as cropping methods, windbreaks and shelterbelts, soil-water management, and tillage operations.

2.3 Wind erosion Modeling

Measuring wind erosion is crucial for gaining a comprehensive understanding of its underlying mechanisms, assessing its environmental impact, predicting when and where it might occur, and evaluating the effectiveness of conservation practices. The study of wind erosion began in the 1940s, primarily through field and laboratory investigations aimed at discerning the influence of individual factors on this complex process (Fryrear et al., 1999).

Wind erosion models emerged as invaluable tools for shedding light on this phenomenon and quantifying soil particle movement across various temporal and spatial scales (Bhuyan et al., 2002; Boardman and Poesen, 2006). These models offer essential insights into how different factors contribute to wind erosion, facilitating monitoring and forecasting while supporting the implementation of conservation policies (Bhuyan et al., 2002).

Wind erosion models come in diverse forms, each with varying levels of complexity, input data requirements, and outputs. The suitability of a particular model depends on the specific objectives of its users (Merritt et al., 2003). Additionally, factors such as data availability, model accuracy and validity, model components, and hardware requirements influence the selection of a model for a particular purpose.

The erosion models possess inherent limitations that introduce a degree of uncertainty into the accuracy of its outputs. While initial wind erosion models faced challenges, including high data demands, unrealistic assumptions, and limited validation in different regions, ongoing research and development have led to improved models that offer more accurate estimates of wind-induced soil erosion and suggest effective soil conservation strategies.

Wind erosion models play a pivotal role in comprehensively understanding erosion processes and their associated factors. These models offer valuable insights into the on-site and off-site consequences of wind erosion across various spatial and temporal scales. They are instrumental in estimating soil erosion rates, ranging from small scale local areas to larger geographic regions on a regional and national scale. Additionally, wind erosion models aid in evaluating suitable erosion control strategies (Blanco-Canqui and Lal, 2008a).

The origin of most wind erosion models can be traced back to early research on wind mechanics and dynamics, notably pioneered by Chepil (1945a, 1945b, 1945c). Early investigations primarily focused on climate and soil surface properties as the key determinants of wind erosion mechanics. Chepil (1959) introduced Eq. 2.1 that expanded the theoretical foundation by emphasizing the main factors influencing wind erosion.

$$E = IRKFBWD \ldots\ldots\ldots\ldots\ldots\ldots \text{Eq. 2.1}$$

The components of the Eq. 2.1 include soil cloddiness (I), vegetative material (R), ridge roughness (K), soil abradability (F), wind barrier (B), field width (W), and wind direction (D). Over time, wind erosion models have evolved through a deeper understanding of influential factors (Blanco-Canqui and Lal, 2008a).

These models exhibit various estimation capabilities and utilities, classified into three main categories: empirical, conceptual, and process-based (Merritt et al., 2003). Numerous wind erosion models have been developed, but the focus here is on models designed for diverse applications across different scales and regions.

2.3.1 Wind Erosion Equation and Revised Wind Erosion Equation

Wind Erosion Equation (WEQ) emerged as the initial empirical wind erosion model. It was rooted in the work of Chepil (1959) and aimed to assess annual soil loss based on findings from wind tunnel experiments and field measurements (Woodruff and Siddoway, 1965). As computing technology advanced, WEQ evolved into a highly sophisticated empirical model (Blanco-Canqui and Lal, 2008a; Fisher and Skidmore, 1970).

WEQ served as a critical tool for planning wind erosion control systems and underwent continuous refinement. This progress eventually culminated in the development of the Revised Wind Erosion Equation (RWEQ) by Fryrear et al. (1998). RWEQ was designed to incorporate more extensive information from agricultural fields and enable short-term estimations of soil erosion, including daily and longer-term assessments (Fryrear et al., 1998).

Wind Erosion Equation and Revised Wind Erosion Equation serve as valuable tools for predicting wind-induced soil erosion. These models offer insights into the average wind erosion (E) occurring along a line-transect over wide, exposed, unsheltered, smooth, non-crusted surfaces, typically measured in mass per unit area per year (Fryrear et al., 1999; Woodruff and Siddoway, 1965). In the WEQ model, several factors are considered to estimate the potential annual wind erosion from a field (Woodruff and Siddoway, 1965). Eq. 2.2 below governs this model.

$$E = f(I, K, C, L, V) \quad \ldots\ldots\ldots\ldots\ldots\ldots \textit{Eq. 2.2}$$

E (Mg ha-^{1} yr^{-1}) in Eq. 2.2, represents the average annual soil loss, I denote the soil erodibility factor, *K* represents the soil ridge roughness factor, *C* signifies the climatic factor, and *L* denotes the length of the field factor. The latter can be adjusted for wind protection measures, such as wind barriers, while *V* represents the equivalent vegetative or residue factor.

The factor I is closely linked to the percentage of non-erodible aggregates AGG as shown in Eq. 2.3 below and accounts for knoll erodibility, considering soil topography. Fields with steeper slopes may experience increased wind velocity, affecting the I value (Woodruff and Siddoway, 1965).

$$I = 525(2.718)(0.04\,AGG) \quad \ldots\ldots\ldots\ldots\ldots\ldots \textit{Eq. 2.3}$$

C is an annual climate parameter in an integrated form and has been produced as iso-C value maps which is determined as shown in Eq. 2.4 above where, *U* is the mean monthly wind velocity at a height of 10 m*, ETP_i* is monthly evaporation (mm), *Pi* is monthly precipitation (mm), and *d* is the number of days in the considered months.

$$\mathrm{C}=\frac{di}{100}\sum_{i=1}^{i=12} U\left(\frac{ETPi-Pi}{ETPi}\right) \quad \ldots\ldots\ldots\ldots\ldots \text{Eq. 2.4}$$

The ridge roughness factor *(K*) is calculated based on the ratio of ridge height to ridge spacing, in which the *K* value for a flat, bare and smooth field is equal to 1. *L* factor, measured along the prevailing wind erosion direction and adjusted for any barriers present is the total distance across a given field. *V*, the equivalent vegetative cover factor comes from complex graphs that relates various vegetation types, quantity and crop orientation to a flat small-grain equivalent. RWEQ builds upon the Wind Erosion Equation (WEQ) and integrates empirical and process-based components (Jarrah et al., 2020a).

A number of studies have found good agreement between the yields predicted by RWEQ and the field measurements. RWEQ also has a limited need for input data compared to other models (Borrelli et al., 2017a) thus making it a suitable tool for modelling wind erosion. In this research, a GIS version of RWEQ is utilized to asses quantitatively soil loss by wind erosion over large study areas. The GIS-RWEQ model reproduces the main components of RWEQ in a GIS environment. The Revised Wind Erosion Equation estimates the amount of soil eroded and transported by wind within the first 2-meter height for a specified time period.

RWEQ underwent extensive testing in the Great Plain area (Fryrear et al., 1999), with its input factors originating from both field and laboratory studies (Woodruff & Siddoway, 1965). The model is relatively straightforward, requiring minimal input data, rendering it suitable for upscaling (Zobeck et al., 2000; Youssef et al., 2012; Guo et al., 2013).

Wind serves as the primary driving force in the model, independently of soil type. The model predicts soil loss up to the transport capacity achievable by the wind. The key components of the model include Q_{max} (maximum transport capacity), s (critical field length), WF (weather factor), EF (soil erodible fraction), SCF (soil crust factor), K' (soil roughness factor), and COG (combined crop factors).

The average soil loss (SL) at a specific point in the field is also calculated (Fryrear et al., 2000). The model estimates the mass transport (Qx (Kgm-1)) at a specific downwind distance (x (m)) away from the upwind border as shown in Eq. 2.5 below. In the Eq. 2.5 Q_x is the mass transport at distance x (kg/m). Q_{max} (which is obtained from Eq. 2.6) is the maximum transport capacity (kg/m), which represents the maximum amount of soil that can be transported by the wind. x is the downwind distance (m) from the upwind border of the field. s (which is obtained from Eq. 2.7) is the critical field length (m), which is the distance at which 63% of the maximum transport capacity is reached.

$$Qx = Qmax * \left[1 - e^{\left(\frac{-x}{s}\right)^2}\right] \ldots\ldots\ldots Eq.\ 2.5$$

$$Q_{max} = 109.8 * CE * EF * SC * K' * VC \ldots\ldots\ldots \text{Eq. } 2.6$$

$$S = 150.71 * CE * EF * SC * K' * VC\text{^}0.371 \ldots\ldots \text{Eq. } 2.7$$

The above Eq. 2.6 and Eq. 2.7 of determining the maximum transport capacity and critical field length, *CE* is the Climate erosivity factor; *EF* is the soil erodible fraction; *SC* is the soil crust factor; *K*' is the soil roughness factor; *VC* is a combined crop factor. The equation for the average soil loss (SL) at a specific point (x in meters) in the field is given as follows in Eq. 2.8.

$$SL = [2x / (s^2)] \times Q_{max} \times e^{(-x/s)2} \ldots\ldots\ldots\ldots\ldots Eq.\ 2.8$$

Where: *SL* is the average soil loss (kg/m^2) at the specified point; x is the downwind distance (m) from the upwind border of the field; s is the critical field length (m), which is the distance at which 63% of the maximum transport capacity is reached. Q_{max} is the maximum transport capacity (kg/m), representing the maximum amount of soil that can be transported by the wind.

The proposed GIS-based version of the RWEQ model, called GIS-RWEQ, adopts a spatially distributed approach based on a grid structure. The process-based modelling approach is governed by the eroding capacity of wind and the inherent potential of the land to be eroded. Diving deep to individually focus on these factors in order to have an understanding of each factor and see how they individually contribute to wind erosion.

The Climatic Erosivity factor (CE), also known as the Weather Factor (WF), quantifies the influence of climate on the wind erosion process, taking into account wind speed and soil moisture conditions. It is the measure of climatic tendency to produce conditions conducive for wind erosion. It is calculated using Eq. 2.9 below. In Eq. 2.9, CE is the Climatic Erosivity (Weather Factor); u_i is the monthly mean wind speed for month I; PET_i is the potential monthly evapotranspiration for month I; P_i is the total precipitation for month I; d_i is the total number of days in month i.

$$CE = \frac{\left(\frac{1}{100}\right) * \sum_{i=12}^{i=1} ui * \frac{(PETi - Pi)}{PETi}}{\frac{1}{di}} \dots\dots\dots Eq.2.9$$

The Erodibility Fraction factor (EF) is a parameter that show the soil properties effect on erodibility factor. These properties portray the ability of soil particles to resist transportation from wind. It is determined using a multiple regression equation proposed by Fryrear et al. (2001), which predicts the wind-erodible fraction of soils based on their texture and chemical properties, as shown in Eq. 2.10 below. In the equation, Sa is the Soil sand content; Si is the Soil silt content; SC is the Ratio of sand to clay contents; OM is the Organic matter content; $CaCO_3$ is Calcium carbonate content.

$$EF = \frac{(29.09 + 0.31Sa + 0.17Si + 0.33Sc - 2.59OM - 0.95CaCO3)}{100} \dots\dots\dots Eq.2.10$$

Soil crust refers to a thin, consolidated layer at the soil surface that is denser and mechanically stable. The soil crust is more resistant to abrasion by blowing soil and erodes at a slower rate compared to loosen bare soil beneath it (Fryrear et al., 2001). In arid regions, soil crust plays a crucial role in reducing wind erosion through abrasion. The Soil Crust (SC) factor has been used to estimate the influence of soil crust on the susceptibility of soils to wind erosion (Borrelli et al., 2017; Fenta et al., 2020). The SC-factor is computed based on the inverse abrasion coefficients related to clay and organic matter content, as shown in Eq 2.11 below. In the equation, *CL* is the Clay content of the soil; *OM* is the Organic matter content of the soil.

$$SC = \frac{1}{(1 + 0.0066(CL)^2 + 0.21(OM)^2)} \ldots\ldots\ldots\ldots Eq.2.11$$

Vegetation Cover *(VC)* factor is the percentage of ground covered with non-erodible plant material. Vegetation cover provides a protective shield for soil against the erosive effects of wind. Field studies conducted by Fryrear et al. (2001) have demonstrated that having 20% vegetation cover on a field can result in a 50% reduction in soil erosion compared to completely bare surfaces. In contrast, soils that are permanently bare or left bare in agricultural fields are highly vulnerable to wind erosion. VC is obtained using the Eq.2.12 below. In the equation, NDVI is the Normalized Difference vegetation index; $NDVI_{soil}$ is the Pure bare land pixel value; $NDVI_{veg}$ is the Pure vegetation pixel value

$$VC = \frac{\mathrm{NDVI} - \mathrm{NDVIsoil}}{\mathrm{NDVIveg} - \mathrm{NDVIsoil}} \ldots\ldots\ldots\ldots Eq.2.12$$

Surface Roughness factor *(K)* is the landscape condition that affect the wind erosion process by dissipating the erosive force of wind. This information can be derived from the Copernicus Climate Change Service (C3S), which provides Intermediate Climate Data Records (ICDRs) for various Essential Climate Variables (ECVs), including land cover. The C3S LC project supplies global land cover maps at a spatial resolution of 300 meters, stored in NetCDF file format and comprising 23 land classes. To obtain this, the land cover classes are reclassified where, highest value are given to areas with lowest roughness and the vice versa.

2.4 Regional Studies on Wind Erosion

Regional studies on wind erosion have played a pivotal role in enhancing the understanding of this complex phenomenon. Zobeck et al. (2000) conducted extensive research on wind erosion prediction using the Revised Wind Erosion Equation (RWEQ), providing valuable insights into soil loss due to wind erosion. Youssef et al. (2012) focused their regional study on pastures in northwestern Oklahoma, developing a wind erosion prediction model tailored to the specific conditions of the region. Borrelli et al. (2017) adopted a quantitative spatially distributed modeling approach to assess soil loss from wind erosion across European agricultural soils, demonstrating the applicability of the RWEQ model at a larger scale.

Fenta et al. (2020) examined soil erodibility and soil crust formation rates in the Chihuahuan Desert, USA, shedding light on the susceptibility of arid regions to wind erosion. Furthermore, Fryrear et al. (2001) delved into the wind erodibility of soils in the Great Plains of the USA, providing crucial data for understanding wind erosion dynamics in this region.

2.5 Land Use Land Cover Impact on Wind erosion

Land Use and Land Cover Changes (LULC) are critical global concerns driven by intensifying human activities. These changes have far-reaching environmental impacts, affecting climate, biodiversity, and ecological services. LUCC can lead to ecosystem degradation, causing reductions in land resources, soil quality, and biodiversity. The consequences of LUCC pose significant challenges to sustainable development.

Wind erosion is a critical factor that impacts soil conservation services, leading to land degradation and threatening socio-economic development. Land use and land cover (LULC) changes in Baringo County have profoundly affected wind erosion dynamics. These changes encompass deforestation, expansion of agricultural areas, and shifts in land management practices, collectively influencing the region's susceptibility to wind erosion.

The diminishing vegetation cover due to deforestation and overgrazing, weakens the protective shield against wind erosion. The loss of natural vegetation exposes soil surfaces, making them more susceptible to wind erosion. In parallel, the expansion of arable land and the resultant soil disturbance exacerbate erosion risks. The combination of reduced vegetation cover and increased soil vulnerability amplifies the potential for wind erosion.

Baringo County's arid and semi-arid climate further compounds the impact of LULC changes on wind erosion. These environmental conditions create an environment where soil is more prone to erosion. As land degradation accelerates due to human activities, including land clearance for agriculture, it triggers a cycle of increased wind erosion potential.

Moreover, the disruption of soil crust, which acts as a protective layer, is a direct consequence of certain LULC changes. Activities such as agriculture and construction can disturb this soil crust, leaving the underlying soil exposed and susceptible to wind erosion. These disturbances add another layer of complexity to the wind erosion dynamics in the region.

2.6 Efficiency of mitigation measures

Windbreaks, often referred to as shelterbelts, have a long history of use in agriculture. Their primary purpose is to reduce wind speeds and protect crops from wind damage and soil erosion. These vegetative barriers can also influence the atmospheric, soil, and plant environments within and around cropland, contributing to a more stable and productive agricultural ecosystem (Vigiak et al., 2003; Cleugh, 1998; Wiesmeier et al., 2018).

Recent studies have highlighted their positive impact on crop yields, further emphasizing their importance in agroforestry systems (Bennell and Verbyla, 2008; Zheng et al., 2016). Efforts to understand the aerodynamics and effects of windbreaks have been ongoing, employing various methods such as wind tunnel experiments, in situ observations, and numerical simulations (Bitog et al., 2012; Liu et al., 2018; Torita and Satou, 2007).

Wind tunnel experiments for instance, have estimated drag coefficients and aerodynamic porosity, aiding in comprehending how windbreaks influence wind flow (Guan et al., 2003; Liu et al., 2018). While field experiments provide insights into real-world windbreak dynamics, they face limitations due to unstable weather conditions and logistical constraints. This has led to the exploration of alternative methods, such as remote sensing (RS) and geographic information systems (GIS), to assess windbreak efficiency.

Remote sensing platforms have enabled the identification and analysis of windbreaks across large landscapes, enhancing our ability to evaluate their continuity and structural characteristics (Wiseman et al., 2009; Deng et al., 2013). Additionally, remote sensing data have been used to estimate parameters related to windbreak efficiency, providing valuable information at different spatial and temporal scales (Deng et al., 2017; Yang et al., 2017).

The friction velocity reduction factor, f_{xh}, is a static parameter that reflects the wind protection efficiency of windbreaks based solely on their structural characteristics. *xh* represents the distance from the windbreak barrier and is a spatial variable. The given equations, (Eq. 2.13) and coefficients (Eq. 2.14a,2.14b,2.14c,2.14d) are used to calculate the friction velocity reduction factor, f_{xh}. Wind porosity(*Θ)* is calculated from the optical porosity (θ_0), windbreak average width (*w*) and barrier height (*h*) as shown in E.q 2.1.

$$f_{xh} = 1 - e^{(axh^2)} + b \times e^{((-0.003(xh+c)^d)} \dots\dots\dots\dots Eq.2.13$$

$$\begin{aligned} a &= 0.008 - 0.17\theta + 0.17\,\theta^{1.05} \dots\dots\dots\dots (a) \\ b &= 1.35 - e^{(-0.5 \times \theta^{0.2})} \dots\dots\dots\dots\dots\dots\dots (b) \\ c &= 10 \times (1 - 0.5 \times \theta) \dots\dots\dots\dots\dots\dots\dots (c) \\ d &= 3 - \theta \dots\dots\dots\dots\dots\dots\dots\dots\dots\dots\dots\dots (d) \end{aligned} \quad \dots\dots\dots Eq.2.14$$

$$\Theta = \Theta_0 + 0.002 \times \frac{w}{h} \dots\dots\dots\dots\dots\dots\dots\dots\dots\dots\dots\dots\dots Eq.2.15$$

The distribution of f_{xh} can then be mapped, and the efficiency of wind protection for windbreak evaluation can be realized based on GIS a platform. This also helps to give a visual distribution of varying scales of efficiency. Taking a look at these structural parameters that are used to calculate the frictional velocity reduction factors individually.

2.6.1 Windbreak Average Width

The width of a windbreak is a critical structural parameter that directly influences its effectiveness in reducing wind speed. Liu et al. (2018) conducted field measurements and numerical simulations to show that wider windbreaks tend to provide more effective wind protection. They found that the width of the windbreak significantly affected the reduction in wind speed on the leeward side. Wind tunnel experiments were used to study the impact of windbreak width on wind speed reduction. Bitog et al. (2012) concluded that increasing windbreak width led to a more significant reduction in wind speed and turbulence intensity.

2.6.2 Optical Porosity

Optical porosity in this context is the measure of how much wind can pass through the windbreak. It is closely related to the density and arrangement of the vegetation within the windbreak. From investigations of the relationship between windbreak porosity and wind speed reduction, Loeffler et al. (1992) found that windbreaks with lower porosity (denser vegetation) provided more effective wind protection by reducing wind speed. Optical Porosity is estimated from spectral data obtained from a satellite imagery. The Eq. 2.16 provided below is a common method for estimating optical porosity.

$$h = -0.105 \times PCA1 + 6.275 \ldots\ldots\ldots\ldots \text{Eq. 2.16}$$

The Eq. 2.16 *has PCA1* as the first principal component derived from spectral data; *SR* is the Simple Ratio calculated from spectral bands; *w* is the windbreak width. Optical porosity is very important in understanding the wind protection provided by windbreaks and it has a significant linear relationship with windbreak structural parameters.

2.6.3 Barrier Height

Barrier height, often represented by the average tree height in the windbreak, is another crucial structural parameter. Taller windbreaks tend to provide better protection against high winds. From field measurements conducted by Wang and Takle (1996) to study the effects of windbreak height on wind reduction. It was found that taller windbreaks were more effective in reducing wind speed and turbulence.

Correlation analysis was performed to determine the average tree height. From the correlation analysis with vegetation indices, (Yang et al., 2021a) found out that the most related vegetation index was the first principal component, with a correlation coefficient of 0.780. This variable was selected to establish the average tree height estimating model by using the least squares estimation method. The model is shown in Eq 2.17. In the equation, h was the average tree height, which was also the barrier height in this study, PCA1 was the first principal component of the satellite image.

$$h = 0.105 \times PCA1 + 6.275 \quad \text{..... Eq. 2.17}$$

2.6.4 Distance from Barrier

The distance from the windbreak along the wind direction is essential for understanding how wind speed changes as you move away from the windbreak. This parameter helps in assessing the spatial extent of wind protection. Bitog et al. (2012) and Liu et al. (2018) considered the distance from the windbreak to study how wind speed recovers as you move farther downwind. They found that wind speed reductions are most significant close to the windbreak and gradually diminish with increasing distance.

2.7 Research gap

Existing research on wind erosion predominantly focuses on global and regional scales, often overlooking the localized effects and dynamics within specific ecosystems, such as Baringo County in Kenya. This oversight presents a significant research gap, especially given the unique environmental, climatic, and anthropogenic factors that influence soil degradation processes in semi-arid areas. The lack of detailed, long-term studies integrating remote sensing and GIS techniques to evaluate the specific impacts of land use changes, deforestation, and climatic variability on wind erosion rates in this locale underscores the need for targeted empirical research.

Furthermore, the application of the Revised Wind Erosion Equation (RWEQ) model in Baringo County represents a novel approach in this context, highlighting another critical research gap. Previous studies have not adequately explored the model's potential to quantify soil loss due to wind erosion in Kenya's semi-arid regions, nor have they sufficiently correlated these findings with land cover changes over time. This project seeks to bridge this gap by employing RWEQ alongside advanced analytical techniques to provide a comprehensive assessment of erosion susceptibility.

The study opted for the Revised Wind Erosion Equation (RWEQ) primarily due to its flexibility in accommodating the unique environmental and climatic variables of Baringo County. RWEQ offers the adaptability required for customizing key parameters like soil properties, vegetative cover, and climatic factors, ensuring a more precise representation of the region's distinctive conditions. RWEQ's integration with GIS aligns with the study's emphasis on utilizing geospatial technology for the evaluation of localized wind erosion dynamics.

CHAPTER 3: MATERIALS AND METHODS

This chapter shifts the focus to the practical aspects of the study. Section 3.1 dives into the specifics of the study area, describing its geographical features, climatic conditions, and primary land uses. Section 3.2 introduces the data sources utilized and their purpose and role as detailed in Table 3.1. Section 3.3 outlines the methodology, explaining how the study objectives were achieved. Finally, Section 3.3.1.4 presents the soil loss calculation process using the Revised Wind Erosion Equations, ensuring a comprehensive understanding of the approach.

3.1 Study area

Baringo County, situated in Kenya's Rift Valley, encompasses an area of approximately 11,075 Km^2, defined by a mix of arid plains and elevated terrains such as the Tugen Hills and Kerio Valley. Its geographical coordinates position it between latitudes 0.4585° N and 0.8788° S, and longitudes 35.8293° E and 36.2500° E as shown in Figure 3.1. The county's diverse landscape, from the low-lying shores of Lake Baringo to the higher altitudes inland, presents a variety of climatic and ecological conditions that directly impact land use, agricultural practices, and local biodiversity.

The primary land uses in Baringo County include agriculture and livestock rearing, with rainfed farming of maize, beans, and sorghum being prevalent among local communities. Livestock farming, especially cattle herding, forms the backbone of the economy in the rangelands and pasturelands. This agricultural dominance is set against a backdrop of varied land cover, including croplands, forests, wetlands, and water bodies, which contribute to the county's ecological balance and biodiversity.

Climatically, Baringo experiences a semi-arid climate marked by distinct wet and dry seasons, making it susceptible to drought due to erratic and low rainfall averaging between 500 and 800 mm annually. Temperature variations, with daytime temperatures often surpassing 30°C during dry seasons, and the presence of strong winds, exacerbate soil erosion, impacting agriculture and contributing to the county's classification as an arid and semi-arid land (ASAL).

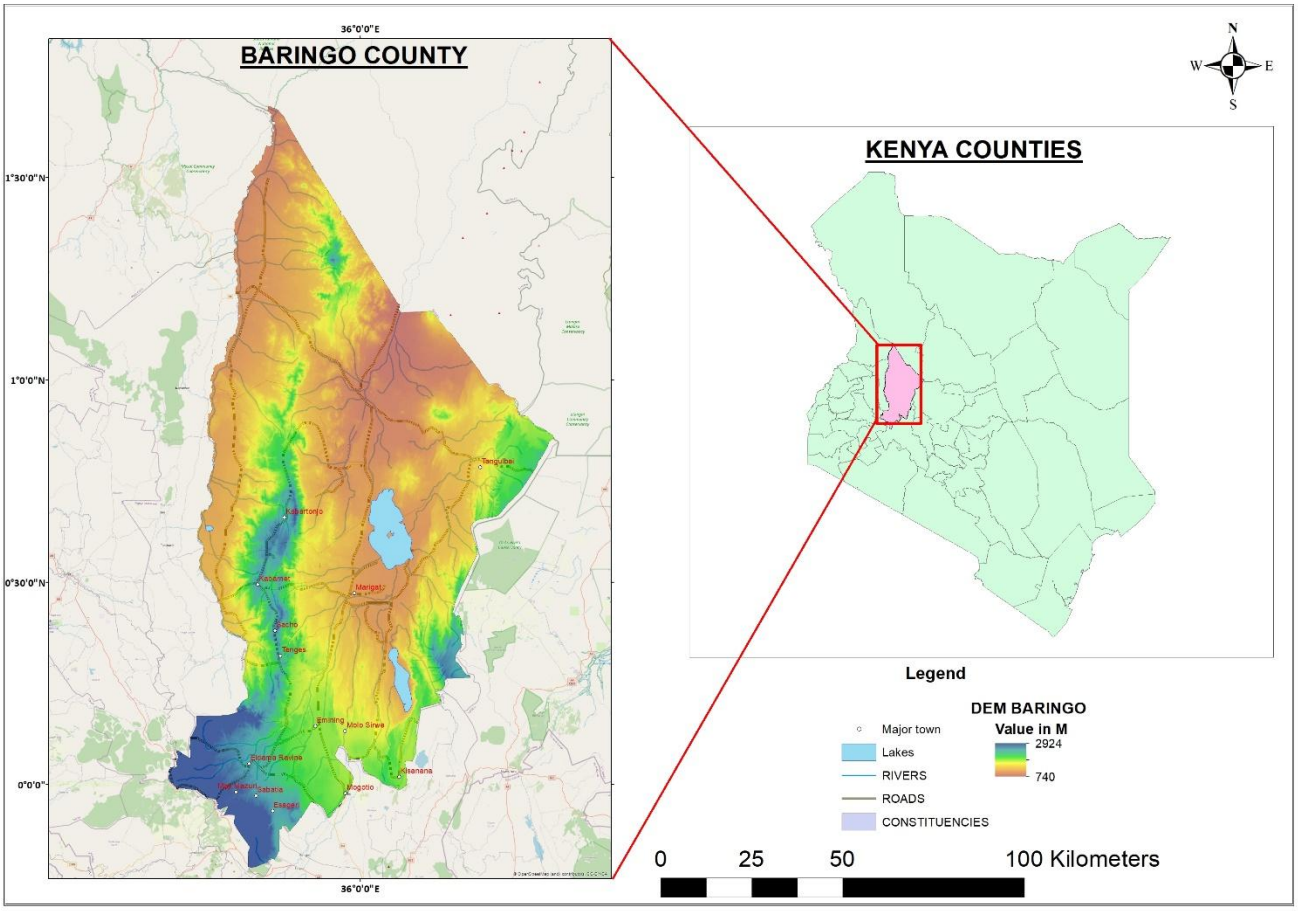

Figure 3.1: Map of Baringo County

Soil diversity in Baringo County reflects its varied topography and climatic conditions, with soils primarily of volcanic origin. In the fertile low-lying areas around Lake Baringo, alluvial soils predominate, while the highlands feature well-drained, loamy soils suitable for diverse agricultural activities. Despite the fertility in some areas, soil degradation, characterized by erosion and nutrient depletion, remains a challenge.

3.2 Data

A compilation of six distinct datasets were used in order to achieve the objectives mentioned, as outlined in Table 3.1. Landsat 5 and 8 data were used to obtain land use and land cover changes at 30 m spatial resolution. Planet-Scope data which has high-

resolution multi-spectral bands, offering a granular view at approximately 3.7 m and facilitating extraction of windbreaks/shelterbelts at a finer scale.

Terra-Climate data is a valuable resource in the realm of climate and hydrological studies, offering a comprehensive dataset spanning from 1958 to 2020. This dataset presents monthly records of climate variables and climatic water balance on a global scale. In this context: Precipitation, Windspeed and Evapotranspiration. The Africa-SoilGrids dataset, originating from ISRIC - World Soil Information, provides a comprehensive insight into soil properties across the African continent, including clay, sand, silt, and organic matter content. This data is derived from soil profile information from across Africa and predicts soil properties at six standard depths.

The Copernicus Climate Change Service (C3S) map dataset offers a comprehensive portrayal of the Earth's land surface, categorizing it into 22 distinct classes. These classifications adhere to the United Nations Food and Agriculture Organization's (UN FAO) Land Cover Classification System (LCCS), ensuring international standards are met in characterizing land cover. Data obtained from SeaWiFS, that is, Angstrom Exponent and Aerosol Optical Depth data were crucial to the study as they were used for validation. This was made possible through dust storm mapping by using the two by-products of SeaWiFS data.

Table 3.1: Data Sources and their roles

DATA	**PURPOSE**	**SOURCE**	**Spatial RESOLUTION**
Landsat 5,8	LULC& Fractional; vegetation cover	USGS	30 m
PlanetScope	Friction Velocity Reduction Factor	Planet	3.7 m
Terra Climate	Climate Erosivity	Climatology lab, UOI	4 Km
Africa Soil Grid	Erodibility Fraction & Soil Crust Factor	ISRIC	250 m
SeaWiFS	Dust Storm Mapping	NASA Ocean Color Web portal	4 Km

Copernicus Land Cover Classes	Surface Roughness	Copernicus	300 m

The datasets were acquired from specified sources as mentioned in Table 3.1. Google Earth Engine and QGIS platform were employed to collect and process the data. Landsat 5 TM images of 1995,2000,2005 and 2010 were collected. Landsat 8 OLI images of 2015 and 2020 were acquired as well. Terra-Climate data for each year of the study period was obtained, narrowing down to the variables needed for wind erosion estimation. Africa Soil-Grid data were collected at multiple depths across the study area. Copernicus Climate Change Service maps for the specific year of the study period were obtained.

The acquired datasets were prepared to ensure consistency and suitability for analysis and to correct for radiometric and geometric errors. All the datasets were clipped to Baringo county, which was the area of interest. Filling was performed, which involved replacing missing or incomplete data with estimated values. This process aimed to create a more comprehensive and usable dataset for analysis. The datasets were resampled so as to obtain a uniform pixel for all the datasets.

The datasets underwent a projection process to ensure their alignment spatially. This crucial step aimed to harmonize the various datasets, making them compatible in terms of their spatial resolutions. By projecting the data, it became possible to seamlessly integrate and analyze information from different sources, enhancing the accuracy and reliability of subsequent analyses related to soil erosion estimation. This spatial and temporal alignment was fundamental to the success of the research project.

Water body masking techniques were applied to the datasets to effectively exclude data originating from water bodies. The purpose of this strategic step was to prevent potential interference from these large water bodies in the results obtained. Simple classification for the water areas was done and a remove water function applied to remove the water areas.

Cloud masking methods were implemented to remove cloud covered areas, ensuring data quality. This was made possible using the PIXEL_QUALITY ASSESSMENT (PIXEL_QA) band. This band allowed for a granular evaluation of each pixel's quality and cloud contamination level. Pixels affected by clouds, shadows, or atmospheric interferences were identified and systematically excluded from the analysis.

3.3 Methodology

The study utilized data collected data from 1995 to 2020, with a focus on analyzing various environmental factors over time. Exceptionally, SeaWiFS utilized data from 2000 to 2010 and PlanetScope used 2023 data. The latter was particularly chosen for its advanced capabilities in Object-Based Image Analysis (OBIA), a technique essential for extracting key parameters needed to calculate the friction velocity reduction factor. This factor is critical for assessing the effectiveness of environmental mitigation measures against wind erosion

Addressing the study's third objective, which was to assess the effectiveness of the implemented mitigation measures, data from different sources and times were strategically utilized. The use of OBIA with the 2023 PlanetScope data allowed for a detailed analysis of the current state and effectiveness of these measures. This approach ensured that the analysis could provide insights into how well the mitigation strategies have worked over time, offering a valuable perspective on environmental management practices.

Additionally, the study made a clear distinction between soil and climatic variables. Soil parameters were considered static, meaning they do not change over time, in contrast to climatic variables, which are subject to temporal variations. This distinction is crucial for the analysis as it highlights the difference in how these variables affect environmental studies. Soil variables, being constant, implied that, the input factors derived from soil parameters were constant throughout the study period. The Figure 3.2 below shows a detailed methodology on how the project was executed in order to obtain the desired objectives.

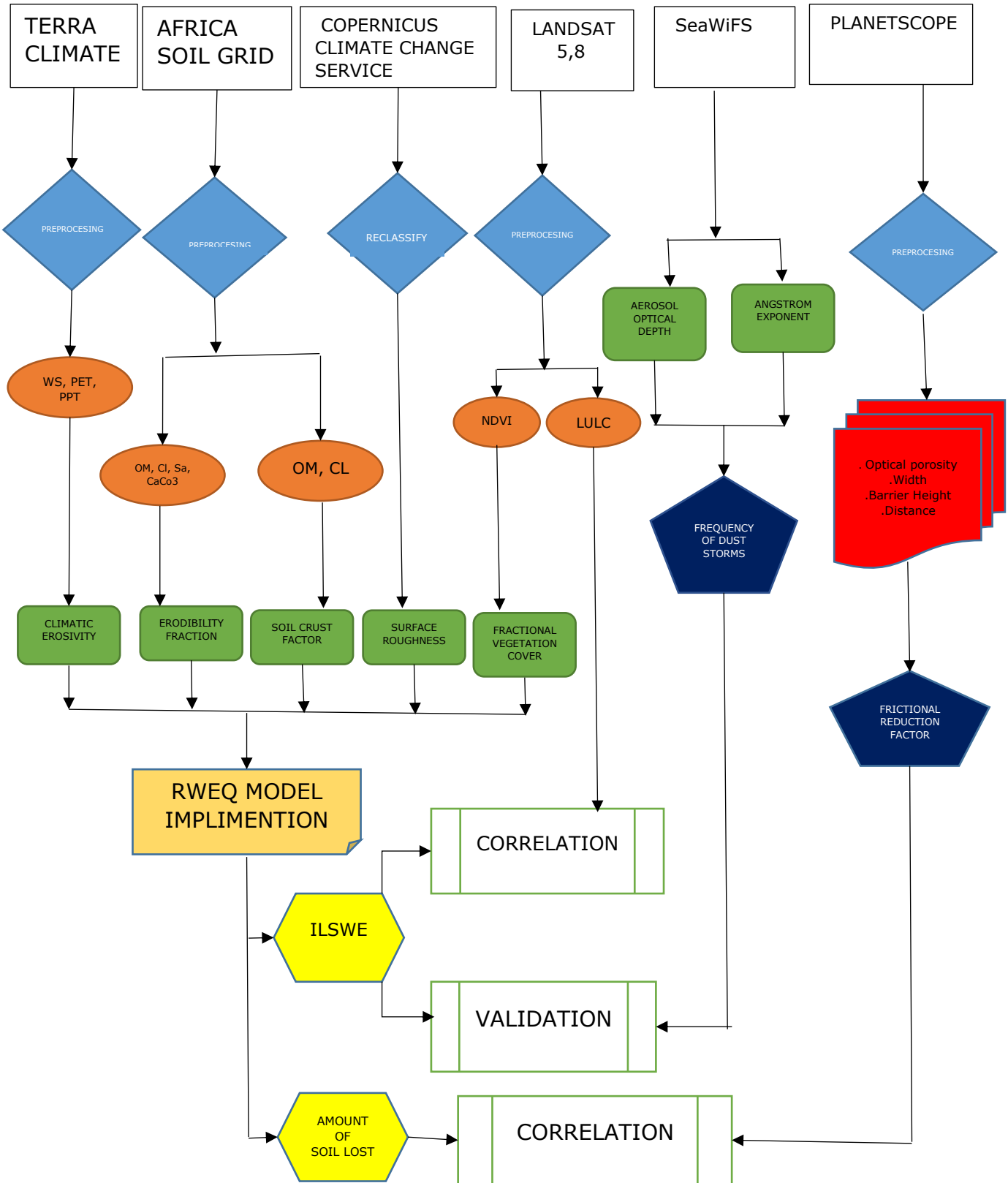
TERRA CLIMATE
AFRICA SOIL GRID
COPERNICUS CLIMATE CHANGE SERVICE
LANDSAT 5,8
SeaWiFS
PLANETSCOPE
PREPROCESING
PREPROCESING
RECLASSIFY
PREPROCESING
PREPROCESING
AEROSOL OPTICAL DEPTH
ANGSTROM EXPONENT
WS, PET, PPT
OM, Cl, Sa, CaCo3
OM, CL
NDVI
LULC
. Optical porosity
.Width
.Barrier Height
.Distance
FREQUENCY OF DUST STORMS
CLIMATIC EROSIVITY
ERODIBILITY FRACTION
SOIL CRUST FACTOR
SURFACE ROUGHNESS
FRACTIONAL VEGETATION COVER
FRICTIONAL REDUCTION FACTOR
RWEQ MODEL IMPLIMENTION
CORRELATION
ILSWE
VALIDATION
AMOUNT OF SOIL LOST
CORRELATION

3.3.1 Soil loss and susceptibility mapping methodology

3.3.1.1 Parameter Calculation

The next step after all the datasets were preprocessed was the calculation of the individual parameters which served as the inputs of the model, namely climate erosivity, Erodibility Fraction, Crustal Erosivity Factor, Surface Roughness and Vegetation Cover.

Climate erosivity factor, relied on the Terra-Climate dataset, covering the study period from 1995 to 2020, which served as the primary data source for climate variables. Monthly meteorological variables, specifically wind speed, precipitation, and potential evapotranspiration data, were extracted from Terra-Climate for each year within the study period. To obtain the annual component of each meteorological variable for a specific year, the mean (average) value was computed. The calculation of climate erosivity (CE-factor) was performed using the formula in Eq. 2.9. The obtained results for the different years are displayed the Figure 3.3 below.

Utilizing data from the Africa Soil-Grid dataset, soil properties, including Soil sand content, Soil silt content, Ratio of sand to clay contents, Organic matter content and Calcium carbonate content were extracted. Erodibility fraction was then computed using the formula and parameters of Eq. 2.10. The obtained erodibility fraction is shown in the Figure 3.4 below.

The crustal erosivity factor was calculated based on available soil data from the Africa Soil grid data, considering the components; Clay and Organic matter using the formula and parameters in Eq 2.11. The obtained crustal erosivity factor of Baringo county is shown in Figure 3.5 below.

The Copernicus Climate Change Service dataset was utilized as the primary data source for surface roughness assessment. This dataset classifies land surface into 22 distinct classes based on the United Nations Food and Agriculture Organization's Land Cover Classification System (LCCS). To obtain the surface roughness factor, the original 22 land cover classes from the Copernicus dataset were reclassified into 5 classes. This reclassification was based on values ranging from 1 to 5, where higher values indicated areas with lower surface roughness as shown in Figure 3.6 below.

Landsat satellite data was employed to assess vegetation cover across the study area. Google Earth Engine (GEE) was used as a platform to access and process Landsat data, enabling the calculation of vegetation-related indices. The primary vegetation index used in this analysis was the Normalized Difference Vegetation Index (NDVI), calculated using Eq. 2.12. The obtained results are as shown in the Figure 3.7 below.

3.3.1.2 Soil Loss Calculation

The necessary parameters for wind erosion modeling; Climate Erosivity (CE), Erodibility Fraction (EF), Soil Crust Factor (SC), Soil Roughness Factor (K'), and Vegetation Cover (VC), using the Revised Wind Erosion Equations, (RWEQ) the process of estimating soil loss was conducted procedurally using the equations from Eq. 2.5 to Eq. 2.8. Maximum Transport Capacity (Q_{max}) was Calculated. Thereafter the Critical Field Length (s) was calculated and lastly the amount of soil loss was computed. The obtained results are displayed in chapter 4, alongside a discussion of the results.

3.3.1.3 Sensitivity mapping

Sensitivity maps of the different factors were calculated and obtained as inputs for executing the calculation. The sensitivity maps for three factors; Climate Erosivity, Erodibility Fraction, and Soil Crust were generated using a unified methodology. Each factor's respective components (Climate erosivity, Erodibility Fraction factor, and Soil Crust factor) serve as inputs for computing sensitivity. The sensitivity maps are derived by applying a common linear fuzzy membership function as shown in Eq 3.2 below. In the equation, x denotes the original value of the factor, and *u* represents the fuzzified value. The terms *lowbound* and *highbound* specify the lower and upper bounds, respectively. The results obtained are as shown in Figures 3.8,3.9 and 3.10.

$$u = \frac{x - low\ bound}{high\ bound - Low\ bound} \quad \text{..... Eq. 3.2}$$

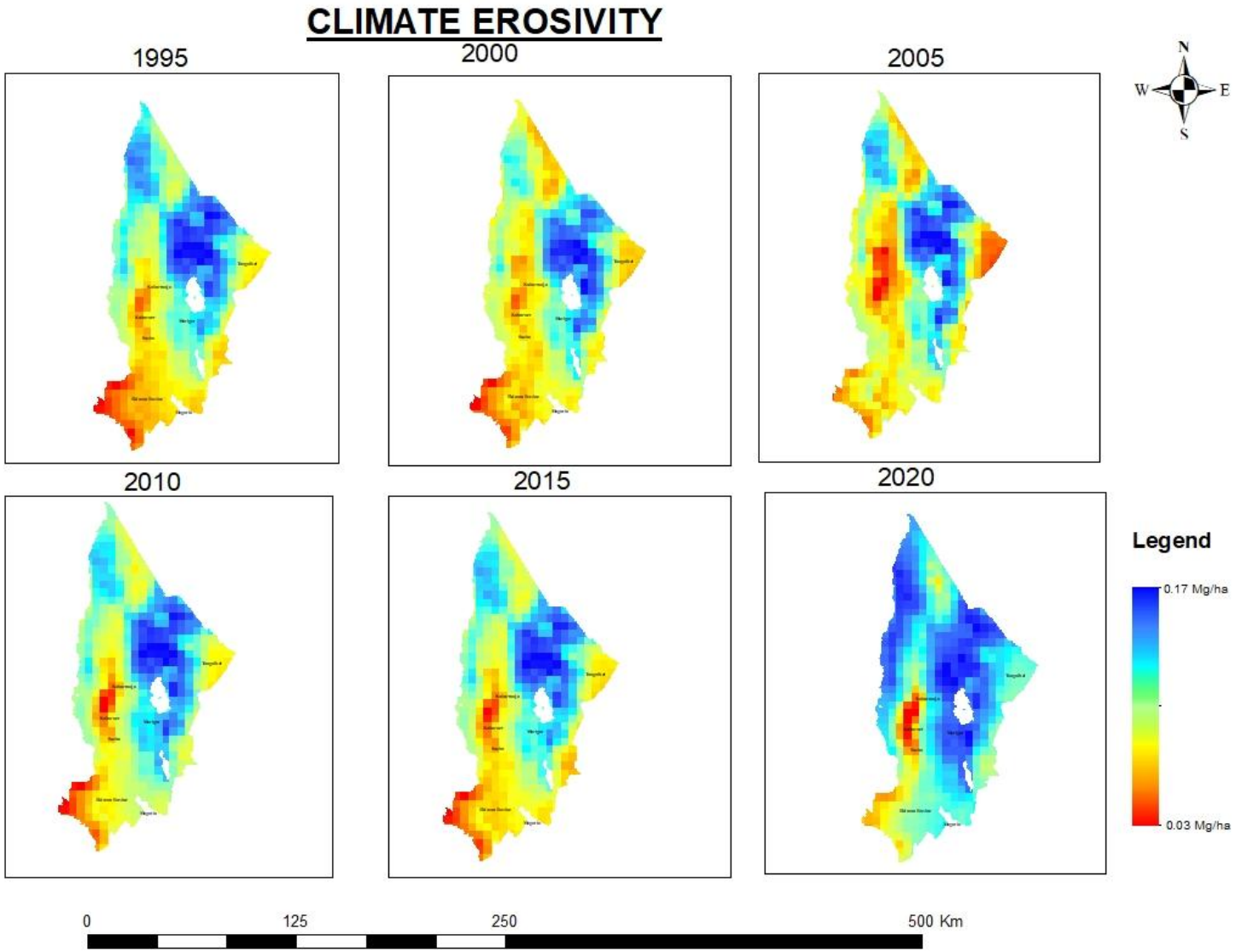

Figure 3.3: Climate Erosivity

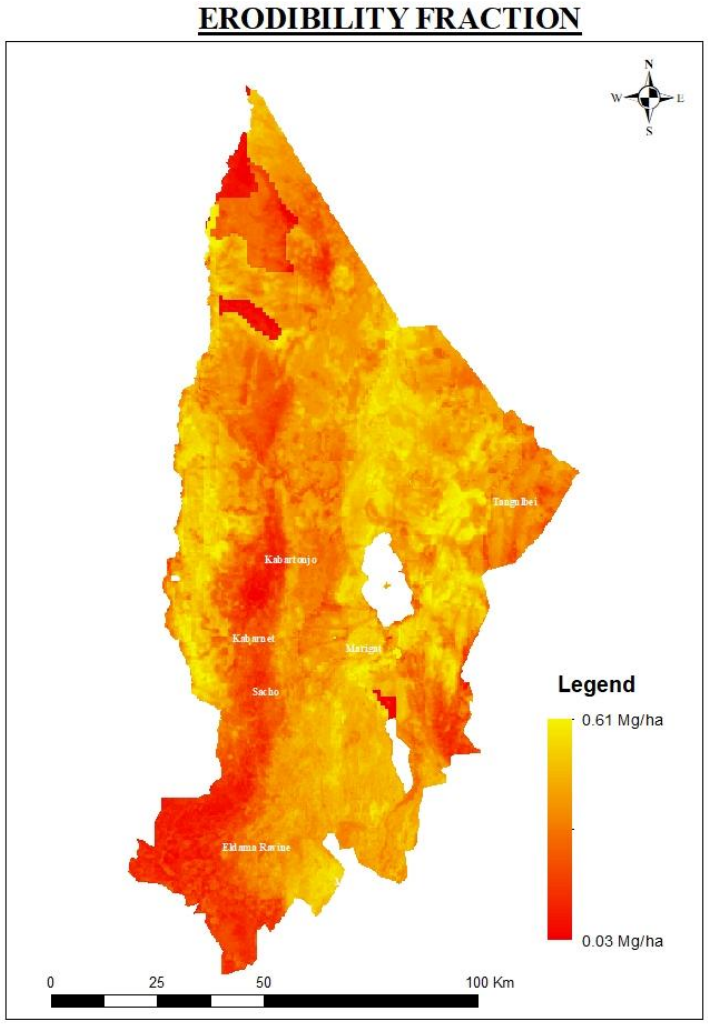

Figure 3.4: Erodibility fraction

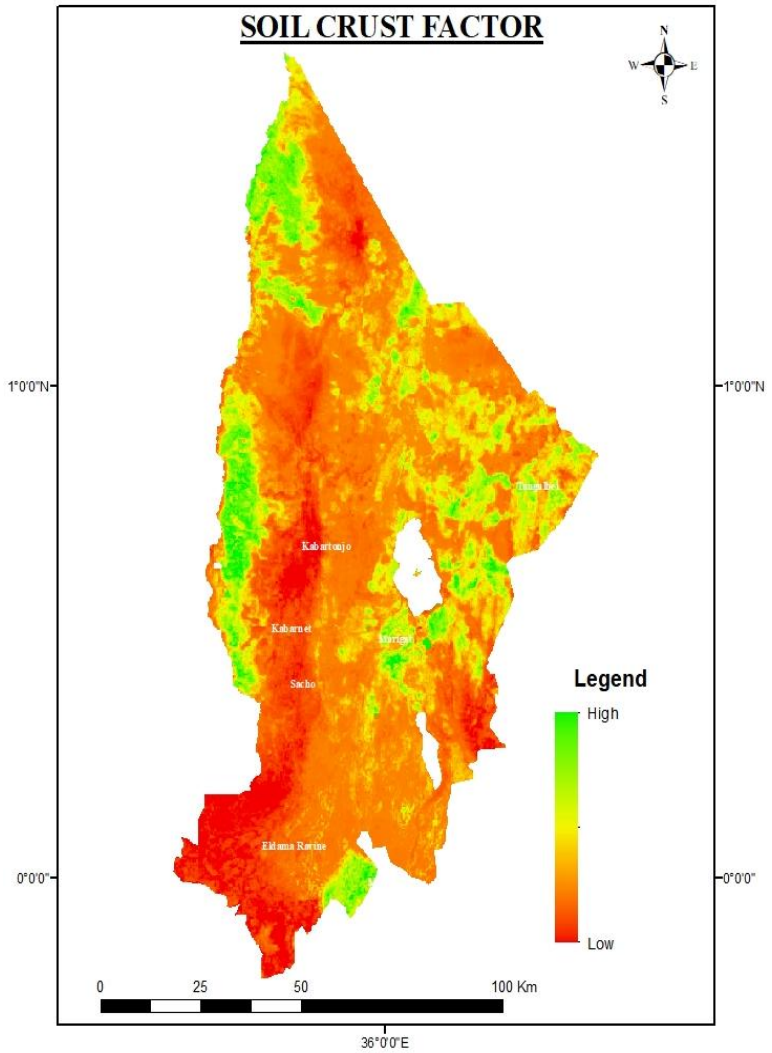

Figure 3.5: Soil Crust Factor

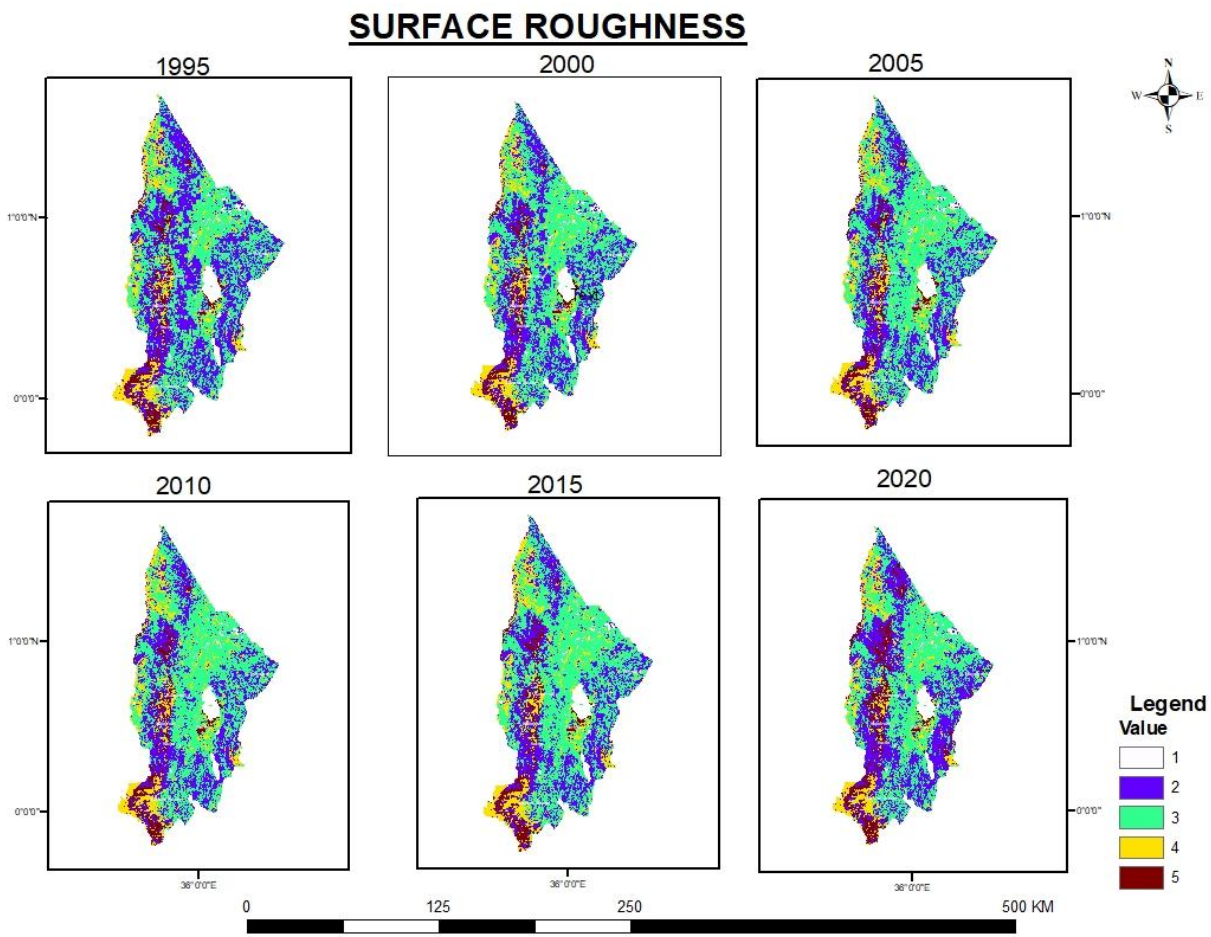

Figure 3.5: Surface roughness

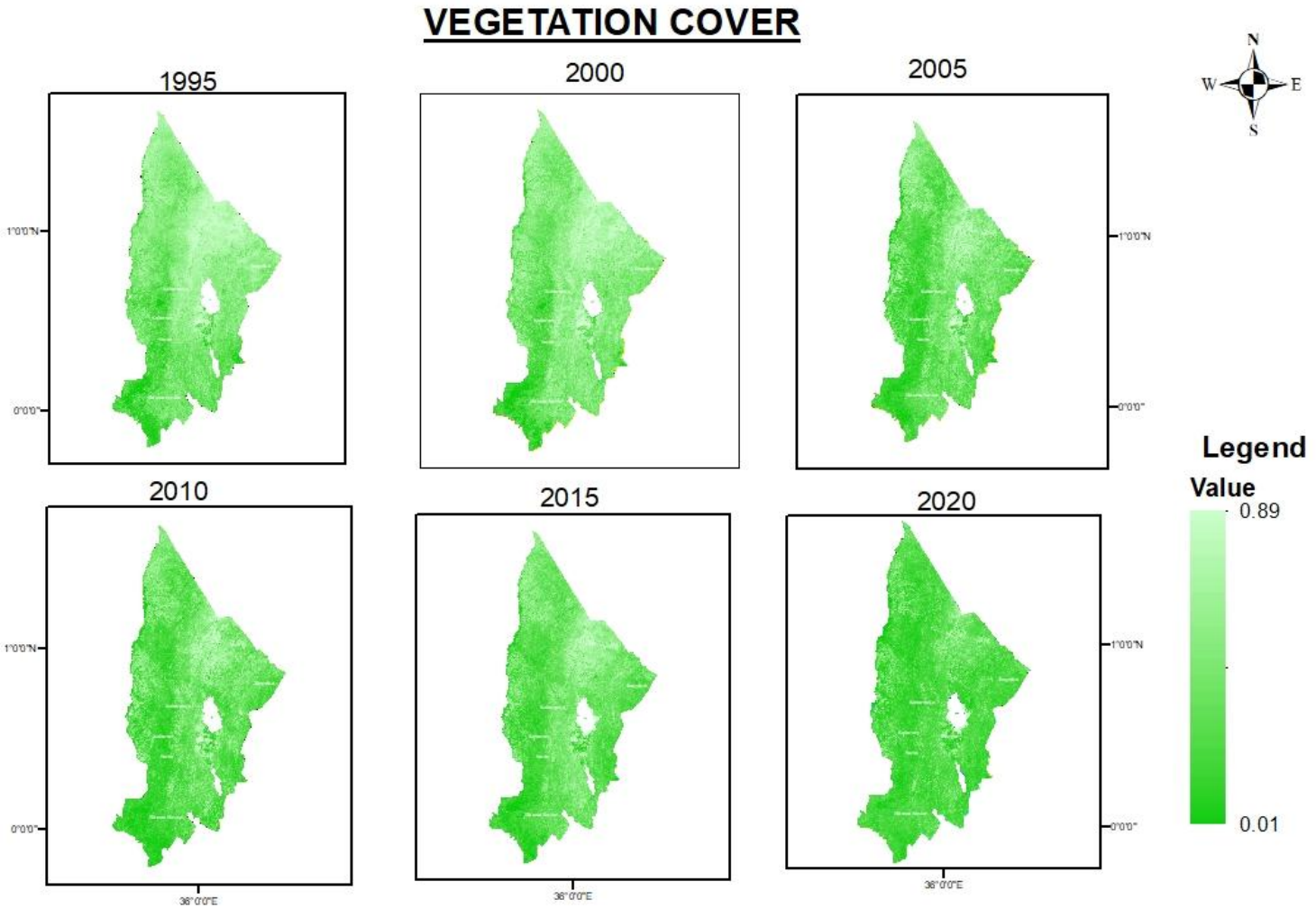

Figure 3.6: Vegetation cover

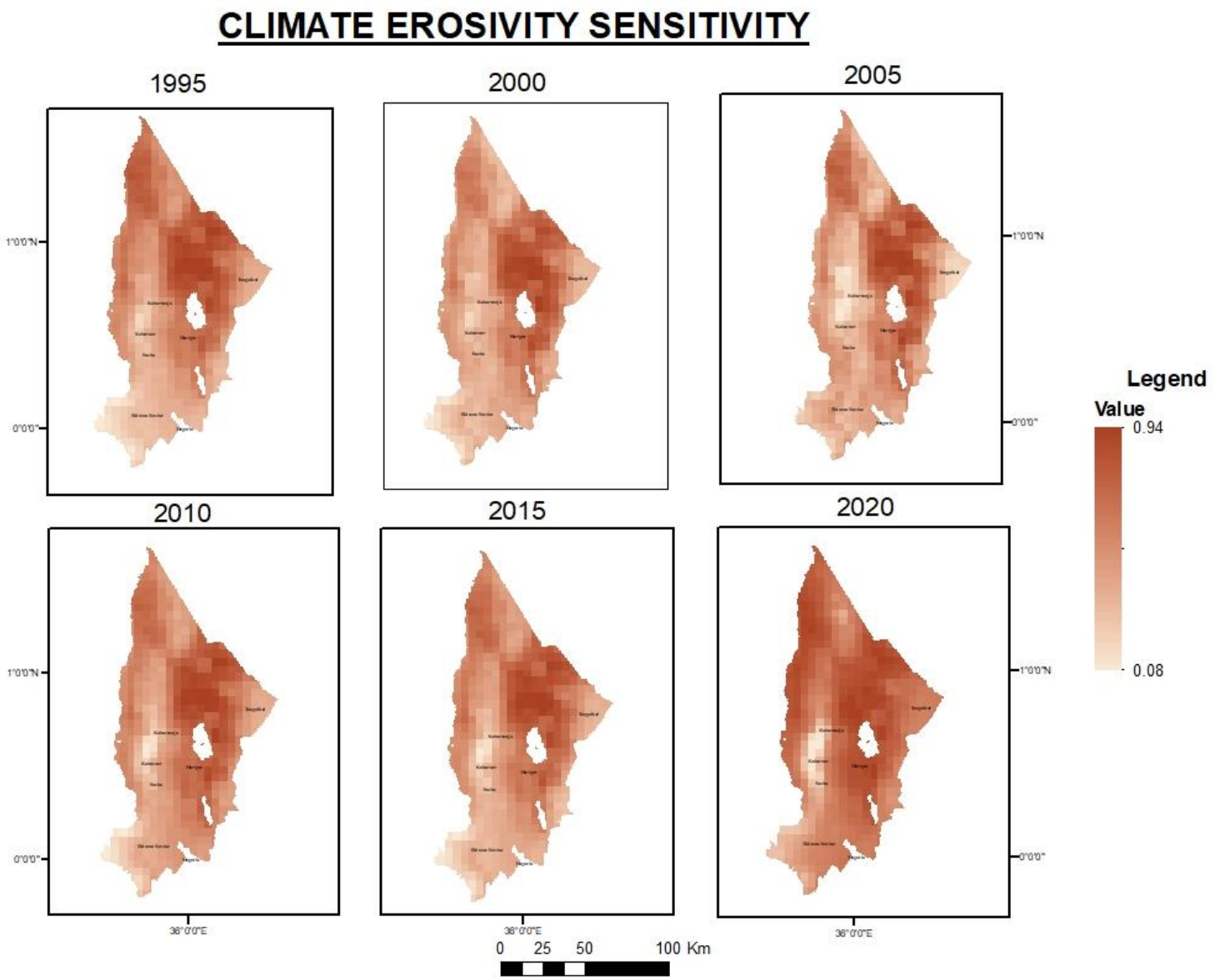

Figure 3.7: Climate Erosivity sensivity

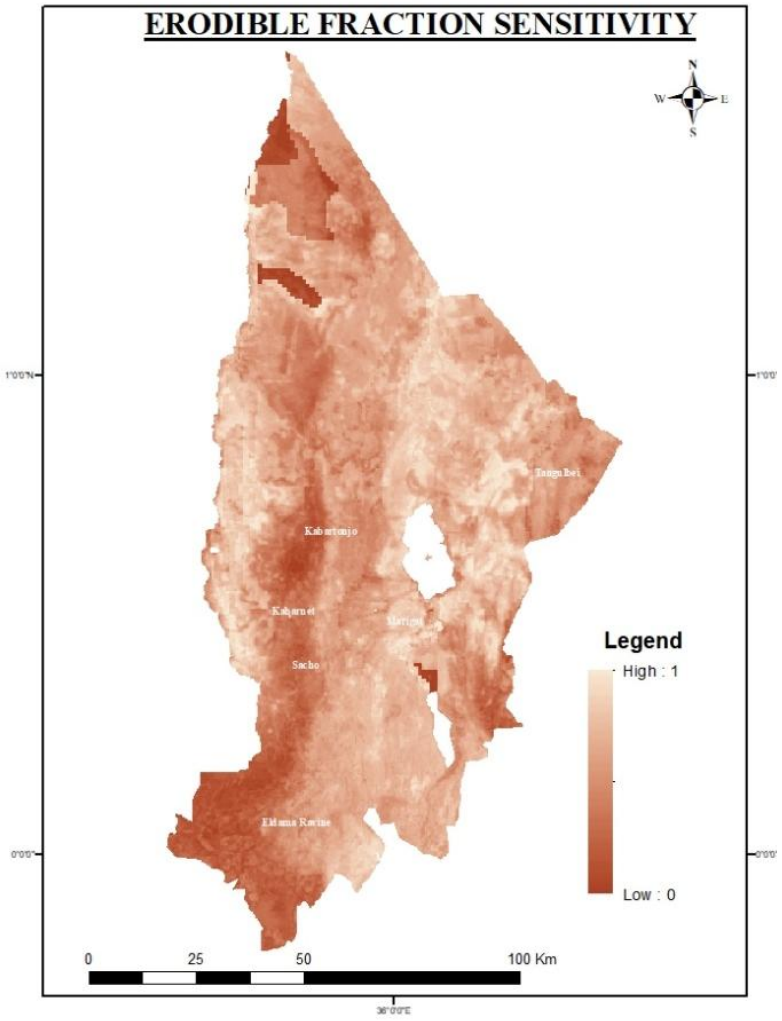

Figure 3.9: Erodibility Fraction sensitivity

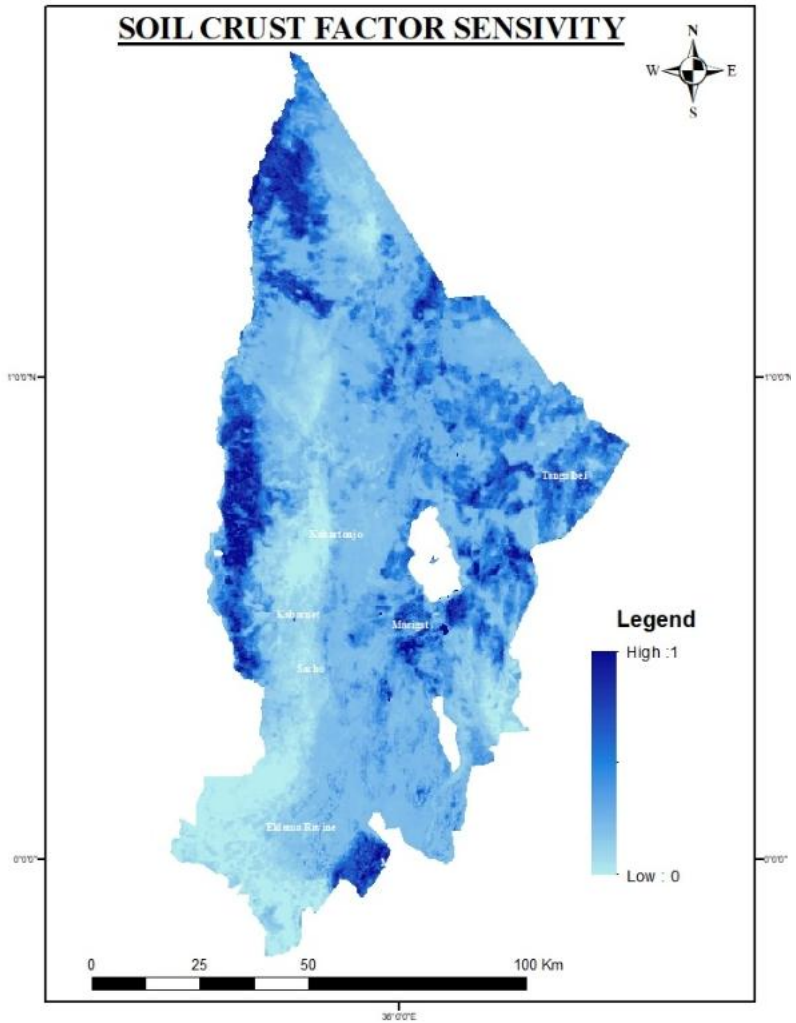

Figure 3.8: Soil crust factor sensitivity

The methodology for computing Vegetation Cover Sensitivity involved assigning a fuzzified value of 0 to areas with significant vegetation cover, and a fuzzified value of 1 to areas with little or no vegetation. This linear, monotonic reduction in sensitivity captured the inverse relationship between vegetation cover and susceptibility. In other words, as vegetation decreases, susceptibility increases, with areas lacking vegetation assigned the highest fuzzified value.

This algorithm incorporates a monotonically decreasing sigmoidal fuzzy membership function, expressed by the Eq. 3.3 below. In the equation, x is the original value and *u* is the fuzzed value. *High* and *Lowbound* define the upper and lower bounds, respectively. The fuzzy membership function is designed such that areas with high surface roughness receive low sensitivity values, while areas with low surface roughness are assigned high sensitivity values. This methodology accounts for the reducing effect of surface roughness on wind erosion, providing a sensitivity map that captures the impact of varying surface roughness on erosive forces.

$$U=\cos\frac{\text{x}-\text{highbound}}{(lowbound-highbound)}*\frac{{P_i}^2}{2} \quad \text{..... Eq. 3.3}$$

3.3.1.4 Index of Land susceptibility to wind erosion

The calculation of Land Susceptibility to Wind Erosion values (ILSWE) was carried out using the multiplicative Eq. 3.4. In the equation, the assessment of land susceptibility to wind erosion is the result of multiplying the wind erosion driving force (CE) by four decreasing factors, namely: EF (Soil Erodible Fraction), SC (Soil Crust), K (a factor not explicitly defined), and VC (Vegetation Cover).

$$\text{ILSWE} = \text{CE} * \text{EF} * \text{SC} * \text{K} * \text{VC} \text{.....Eq. 3.4}$$

Sensitivity maps were created for each of them. These maps assign sensitivity values to pixels within the study area, ranging from 0 (indicating no sensitivity) to 1 (indicating maximum sensitivity). Sensitivity mapping was accomplished through the application of predefined membership functions. The sensitivity map was further reclassified into categories, that is; Very low, low, moderate, high and very high to depict the severity of Baringo to wind erosion. The obtained results of ILSWE are shown in chapter 4 alongside a discussion of the same.

3.3.3 Methodology on land use/cover changes on soil wind erosion

3.3.3.1. Land Use/Land Cover (LULC) change Classification

Landsat 5and 8 data were collected for the years 1995,2000,20005,2010,2015 and 2020, covering the study area. Image classification was performed. In this context, supervised classification method, was employed to categorize land into various land use/cover classes. The classification was categorized into Farmland, Forest, Grassland, water and built-up area. The results of the Land use land cover classification obtained is as shown in Figure 3.11.

Land use/cover change matrix as shown in Table 3.1 below was generated to identify changes in land use/cover classes between 1995 and 2020. This was obtained by, change detection analysis which was performed to compare the classified images from different time periods, identifying and quantifying changes in land use/cover classes over the specified timeframe. The analysis revealed which land use classes had undergone conversion.

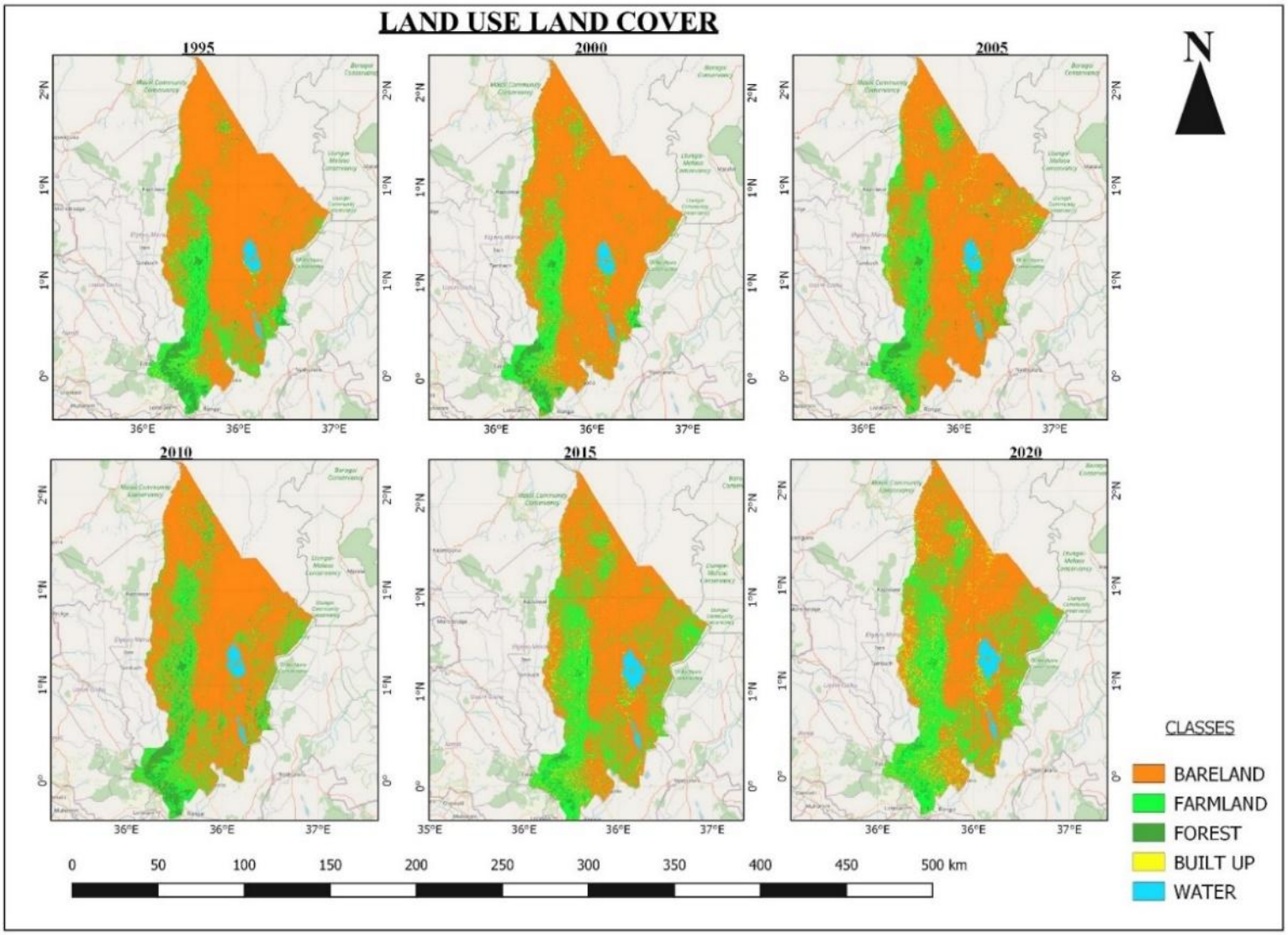

Figure 3.10: Land Use Land Cover

Table 3.1: Land use Transfer Matrix

	LAND CLASS 2000						
		Bareland	Farmland	Forest	Built-up	Water	TOTAL
	Bareland	1887442.19	33527.2966	64.11142	8254.803	513.5794	1929802
	Farmland	83253.3236	114895.661	1970.183	5627.484	325.4529	206072.1
	Forest	5679.93289	17626.1443	30974.48	45.25868	56.65914	54382.48
	Built-up	4448.94643	3958.93694	1.119274	237.0141	53.06873	8699.085
LAND CLASS 1995	Water	216.147632	89.2430119	303.725	32.77901	15343.33	15985.22
	TOTAL	1981040.54	170097.282	33313.62	14197.34	16292.09	2214941
	Land class 2005						
		Bareland	Farmland	Forest	Built-up	Water	TOTAL
	Bareland	1882085.1	84490.4971	4896.429	9330.264	238.2476	1981041
	Farmland	39319.7834	121434.715	8228.194	1041.835	72.75455	170097.3
	Forest	1321.12531	9570.31679	22412.32	1.339417	8.523254	33313.62
	Built-up	7043.14904	6818.87106	22.89879	243.6824	68.73776	14197.34
LAND CLASS 2000	Water	115.38486	170.144511	202.565	39.93702	15764.06	16292.09
	TOTAL	1929884.54	222484.545	35762.4	10657.06	16152.32	2214941
	LAND CLASS 2010						
		Bareland	Farmland	Forest	Built-up	Water	TOTAL
	Bareland	1790084.65	128214.961	8981.644	2348.049	255.2446	1929885
	Farmland	83417.9204	115871.173	21447.15	992.3115	755.9929	222484.5
	Forest	3777.56915	1972.56159	29902.72	1.83376	107.7223	35762.4
	Built-up	9092.36554	1351.79495	3.671762	192.9148	16.31064	10657.06
LAND CLASS 2005	Water	117.045103	1.49505225	54.11134	0.004671	15979.66	16152.32
	TOTAL	1886489.55	247411.986	60389.29	3535.114	17114.93	2214941
	LAND CLASS 2015						
		Bareland	Farmland	Forest	Built-up	Water	TOTAL
	Bareland	1681756.13	100368.985	419.136	6791.147	5600.794	1794936
	Farmland	64184.3279	125126.487	258.3354	10978.57	501.0654	201048.8
	Forest	5153.11932	37355.9413	14445.22	81.54533	58.72005	57094.55
	Built-up	1446.20023	687.645563	1.230208	378.4142	33.10392	2546.594
LAND CLASS 2010	Water	350.846374	138.139004	6.470512	11.21218	16569.36	17076.03
	TOTAL	1752890.62	263677.197	15130.39	18240.89	22763.04	2072702
	LAND CLASS 2020						
		Bareland	Farmland	Forest	Built-up	Water	TOTAL
	Bareland	30815.9629	32846.7487	49.51075	2681.836	172.7009	66566.76
	Farmland	94044.734	140528.105	163.9356	11190.7	501.0654	246428.5
	Forest	7139.49868	23168.7656	8772.129	17.24877	57.00578	39154.65
	Built-up	2319.13751	802.356041	1.162776	378.4607	33.10392	3534.221
LAND CLASS 2015	Water	388.631837	139.261568	6.470512	11.21218	16569.36	17114.93
	TOTAL	134707.965	197485.237	8993.209	14279.46	17333.23	372799.1

3.3.3.2. Analysis of Land Use/Land Cover Conversion and Soil Loss

Previously calculated data on the susceptibility of land to wind erosion over time were used in this analysis. The soil loss data was overlayed with the land use/cover maps for the study period. This allowed for the determination of the severity of soil lost in each land use/cover class for both time periods. Soil loss values were thereafter calculated and recorded for each land use/cover category, quantifying the amount of soil lost within each class.

3.3.4 Evaluating the efficiency of windbreaks methodology

The distance from the barrier along the wind direction in barrier height xh and the structural characteristics of windbreaks θ_0, *w* and *h* should be known in order to estimate the friction velocity reduction factor f_{xh}. To achieve this, PlanetScope imagery from Planet Labs archives was acquired which covered an extensive area of approximately 288 square kilometers, specifically focusing on the Perkerra Irrigation Scheme region.

3.3.4.1 Parameters estimation

The Object-Based Image Analysis (OBIA) methodology was employed in order to extract windbreak width. Pixels within these objects were grouped based on predefined relationships and similarities. Properties such as size, shape, texture, color, and brightness of the images were utilized to create objects. OBIA technology proved efficient in identifying linear wooded strips, and it has been successfully applied in windbreak surveys. Windbreak average width was extracted through object-based image analysis. The extracted windbreak belts are as shown in Figure 3.12 below.

Key parameters such as optical porosity and barrier height were calculated after extracting the width of the windbreaks using specific equations, Eq. 2.19 and 2.20, respectively. To determine the distance from the barrier, the Euclidean distance tool was employed, providing a precise measurement of the spatial separation between observed windbreaks and other relevant geographical features. The results of these parameters are clearly shown in the Figures 3.12,3.13,3.14 and 3.15 below.

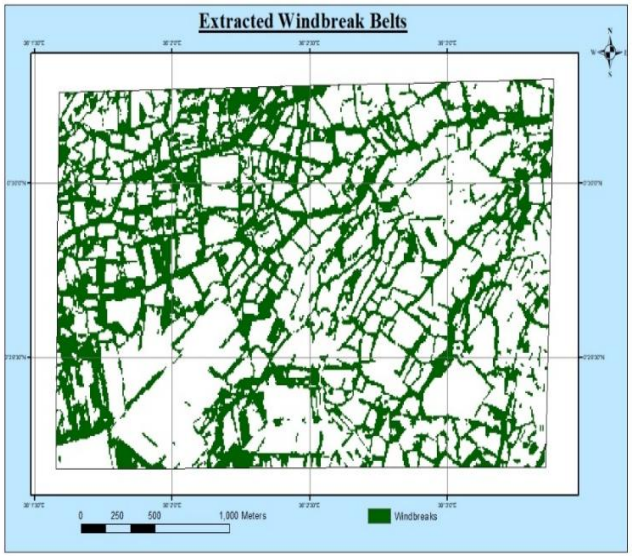

Figure 3.12: Extracted windbreak belts

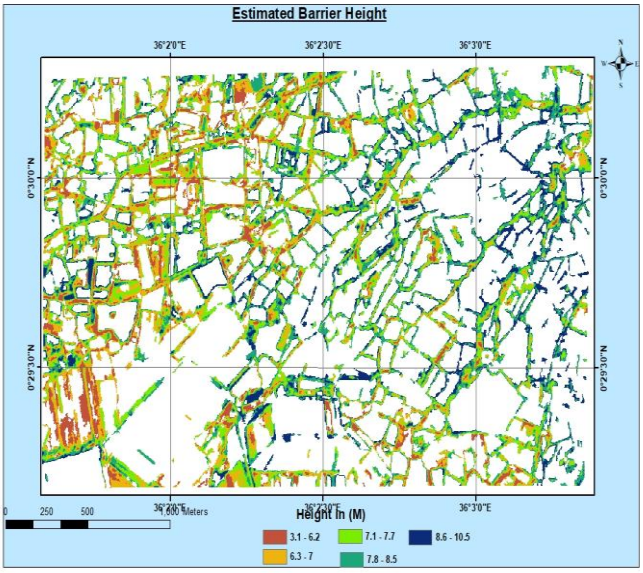

Figure 3.13: Estimated barrier height

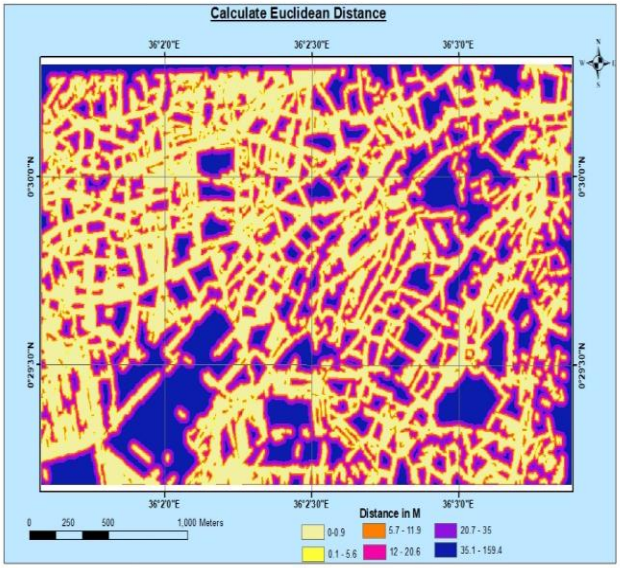

Figure 3.11: Euclidean distance

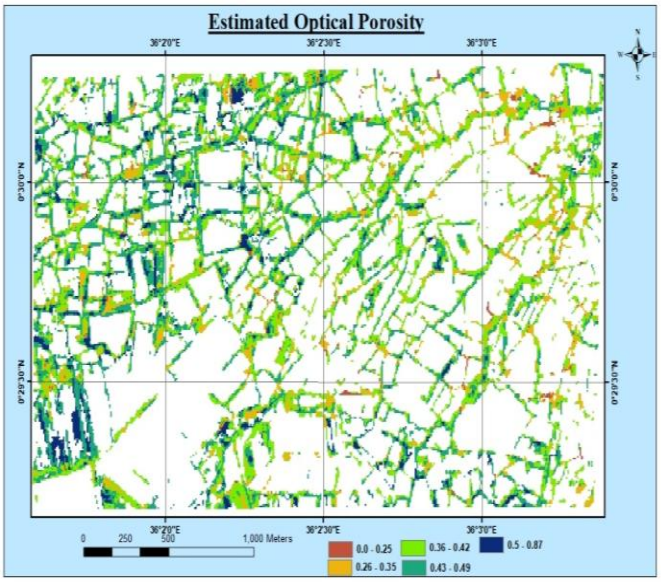

Figure 3.15: Estimated Optical Porosity

3.3.4.2. Friction Velocity Reduction Factor Calculation

The computation of the friction velocity reduction factor, f_{xh}, was achieved through the utilization of the Raster Calculator tool. This process involved applying the mathematical formula described in Eq. 2.13, which takes into account the various windbreak parameters, including windbreak width, estimated optical porosity, and estimated barrier height (equivalent to average tree height). The obtained results are shown in chapter 4 alongside a discussion.

CHAPTER 4: RESULTS AND DISCUSSION

Chapter 4, focuses on presenting the results of the objectives captured in Chapter 2 and engaging in a comprehensive discussion. In Section 4.1, the study unveils the results of its investigations, beginning with soil loss and susceptibility mapping results. These findings shed light on the temporal trends and spatial distributions of soil erosion vulnerability. Additionally, Section 4.1.2 delves into the analysis of land use/cover changes on soil wind erosion, revealing the relationship between human activities and environmental processes. Lastly section 4.1.3 covers the results of the third objective.

The discussion is presented in Section 4.2, where the focus is on interpreting the findings in the context of the study's objectives. Section 4.2.1 explores the implications of soil loss and susceptibility mapping, providing insights into the factors driving erosion vulnerability and potential mitigation strategies. Additionally, Section 4.2.2 delves into the analysis of land use/cover changes, elucidating the complex interplay between human activities and soil erosion dynamics. Furthermore, Section 4.2.3 evaluates the efficiency of windbreaks in mitigating erosion, offering practical insights into the effectiveness of erosion control measures. Finally, a validation process in Section 4.5 assesses the agreement between the wind erosion index and dust storm frequency, enhancing reliability

4.1 Results

4.1.1 Soil loss and susceptibility mapping results

Mean quantity of soil lost, expressed in Kg/Ha, serves as a metric for understanding the impact of wind erosion over the examined period. It serves to quantify the amount of soil that has been lost over the years as a result of wind erosion. The values indicate a consistent rise from 1995 to 2020. Notably, there is a significant increase from 27.90 in 1995 to a peak of 37.73 Kg/Ha in 2005, followed by a fluctuating pattern in subsequent years, with 2020 recording 37.96 g/Ha. The Table 4.1 below shows a summary of the quantity of soil lost in the different years.

Table 4. 1: Average soil lost in Kg/ha

Year	Amount of Soil Lost in Kg/ha
1995	27.89
2000	32.81
2005	37.93
2010	33.44
2015	35.67
2020	36.76

Looking at the results as shown by the maps in Figure 4.1 below, it is evident that; In 1995, a predominant 78% of the county exhibited sediments that were not easily picked up by the wind, while an additional 4% demonstrated low susceptibility. However, by 2000, a notable shift occurred as minimally and mildly susceptible areas decreased to 72% and 4%, respectively. Conversely, highly susceptible areas increased to 24%, signifying an increasing vulnerability to wind erosion.

Further changes unfolded in 2005, with vulnerable sedimentary areas expanding to 29% and the least prone areas dropping to 71%. Notably, from 2005 to 2015, there were fluctuations in areas prone and resistant to erosion, underscoring the dynamic nature of soil erosion processes. Remarkably, the 20-year mark since the study's commencement revealed a significant transformation in the landscape. Areas favoring wind erosion had surged to 32%, indicating an escalated vulnerability, while structurally stable areas dwindled to a coverage of 68%.

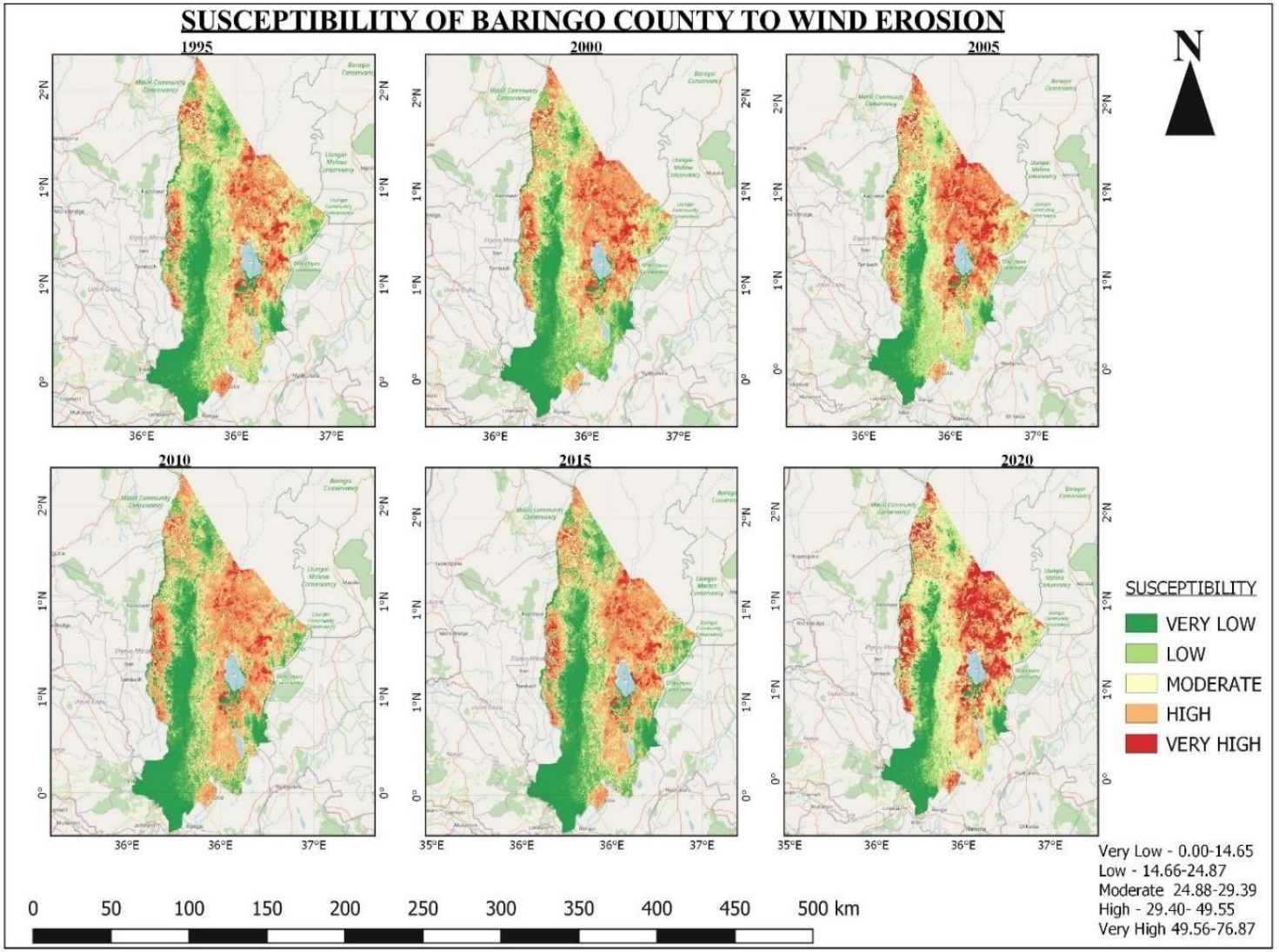

Figure 4.1: Index of Land Susceptibility to wind Erosion

4.1.2 Analyzing the Impacts of land use/cover changes on soil wind erosion results

4.1.2.1 Comparing amount of soil loss and Land Use Land cover classes

Figure 4.2 visually articulates the connection between soil loss and various land cover classes, enabling the straightforward observation of trends in soil loss relative to distinct land cover types over time. From the LULC change matrix as in Table 3.1*, In the* period *1995-2000*, there was a notable conversion of bare land to farmland, totaling 88,097.36 ha. *T*here was a significant decrease in forest cover by 21,239.13 ha, there was also a modest expansion of built-up areas by 5,498.25 ha. During this epoch, the mean amount of soil lost increased from 27.89 to 32.80 kg/ha.

The period between 2000 and 2005, bare land underwent a considerable conversion to other land classes, particularly farmland and built-up areas, totaling 92,257.45 ha. Farmland expanded by 20,697.21 ha, indicating continued agricultural activities. Forest cover experienced a decrease of 18,512.21 ha, Built-up areas continued to increase, reflecting urban development trends. During this epoch the amount of soil lost increased from 32.81 to 37.72 kg/ha

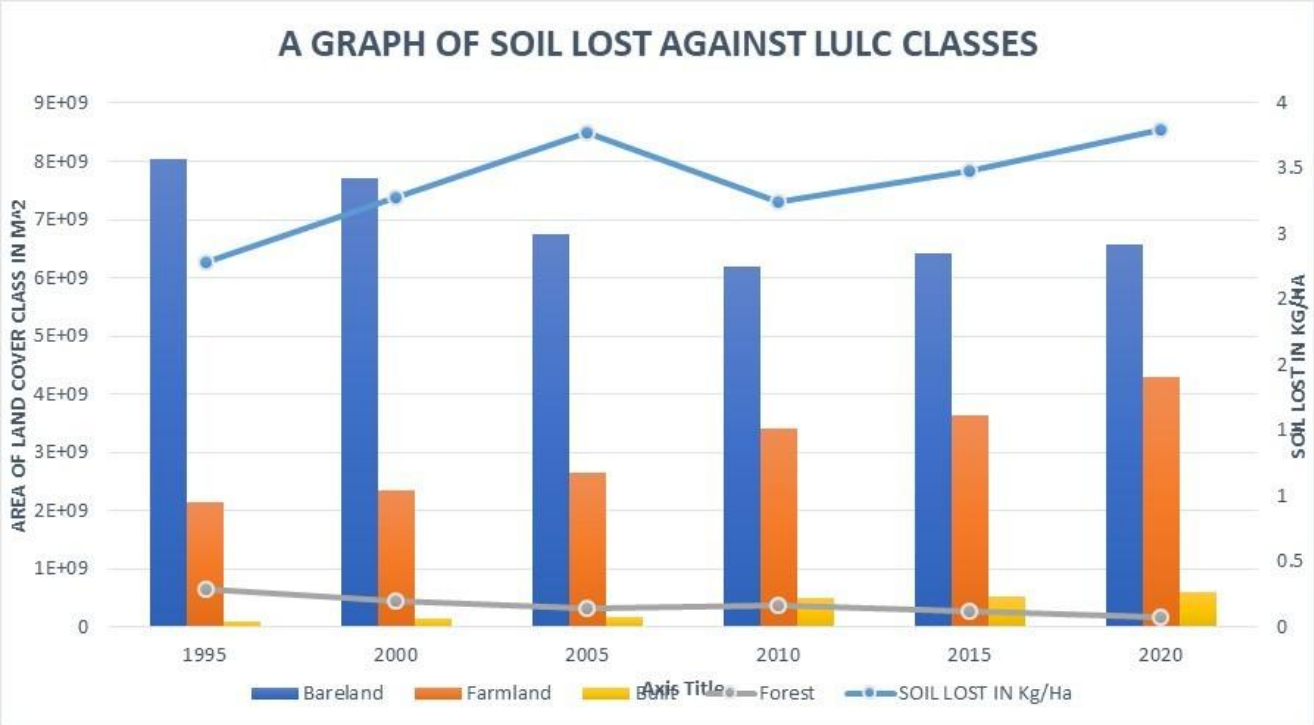

Figure 4.2: A graph of Soil lost against Land cover classes

2005 to 2010 experienced a significant decrease in bare land by 108,095.89 ha, indicating substantial conversion to other land classes, primarily farmland and built-up areas. Farmland expanded notably by 38,146.22 ha, driven by agricultural expansion. Forest cover witnessed a slight increase of 428.21 ha. Built-up areas continued to expand, reflecting urbanization trends. In this epoch soil loss decreased slightly from 37.72 to 33.44 kg/ha

2010 to 2015 experienced an increase in bare land by 13,865.56 ha, indicating significant vegetation loss. Farmland increased notably by 51,341.3 ha, reflecting continued agricultural expansion. Forest cover saw a slight decrease of 707.87 ha, due to deforestation and land conversion. Built-up areas continued to increase, indicating ongoing urban development. This period was marked by an increase in amount of soil lost as a result of erosion from 33.44 to 35.67 kg/ha.

The period between 2015 and 2020 experienced stability in bare land, with a slight increase of only 235 ha. Farmland increased slightly by 2,062.76 ha, indicating continued agricultural expansion. Forest cover decreased by 938.41 ha, due to deforestation efforts and natural regeneration. Built-up areas continued to expand, increasing by 9,179.28 ha, reflecting ongoing urban development trends. This period was marked by an increase in the amount of soil lost from 35.67 to 36.95 kg/ha

4.1.2.2 Comparing land susceptibility to wind erosion and Land Use Land Cover classes

The Table 4.2 below shows the results of the relationship between the land cover classes and the susceptibility categories to wind erosion. In 1995, a predominant 78% of the county exhibited sediments that were not easily picked up by the wind, while an additional 4% demonstrated low susceptibility. By 2000, a notable shift occurred as minimally and mildly susceptible areas decreased to 72% and 4%, respectively. Conversely, highly susceptible areas increased to 24%, signifying an increasing vulnerability to wind erosion.

Table 4.2: LULC and Susceptibility category

Land Class	Very Low (%)	Low (%)	Moderate (%)	High (%)	Very High (%)
Bare land	30.2	45.1	21.0	3.5	0.2
Farmland	40.5	38.0	19.0	2.3	0.2
Forest	55.0	40.0	4.8	0.2	0.0
Built-up	72.0	25.0	2.8	0.2	0.0

Further changes unfolded in 2005, with vulnerable sedimentary areas expanding to 29% and the least prone areas dropping to 71%. This shift pointed towards an increased susceptibility to wind-driven soil dispersal in the county. Notably, from 2005 to 2015, there were fluctuations in areas prone and resistant to erosion, underscoring the dynamic nature of soil erosion processes.

Remarkably, the 20-year mark since the study's commencement revealed a significant transformation in the landscape. Areas favoring wind erosion had surged to 32%, indicating an escalated vulnerability, while structurally stable areas dwindled to a coverage of 68%. This notable increase in highly susceptible areas implied a potential intensification of wind erosion risks over the two decades.

4.1.3 Evaluating the efficiency of windbreaks results

4.1.3.1 Friction Velocity reduction factor

The obtained friction velocity reduction factor values as shown in Figure 4.3 below, ranging from 0.4 to 0.7, indicate a crucial aspect of windbreak efficiency. In this context, higher values of the friction velocity reduction factor showed more effective windbreaks in reducing wind forces and, consequently, minimizing wind erosion. This linear relationship highlights the quantitative measure of windbreak performance, with higher values indicative of increased efficiency in mitigating the erosive impact of wind.

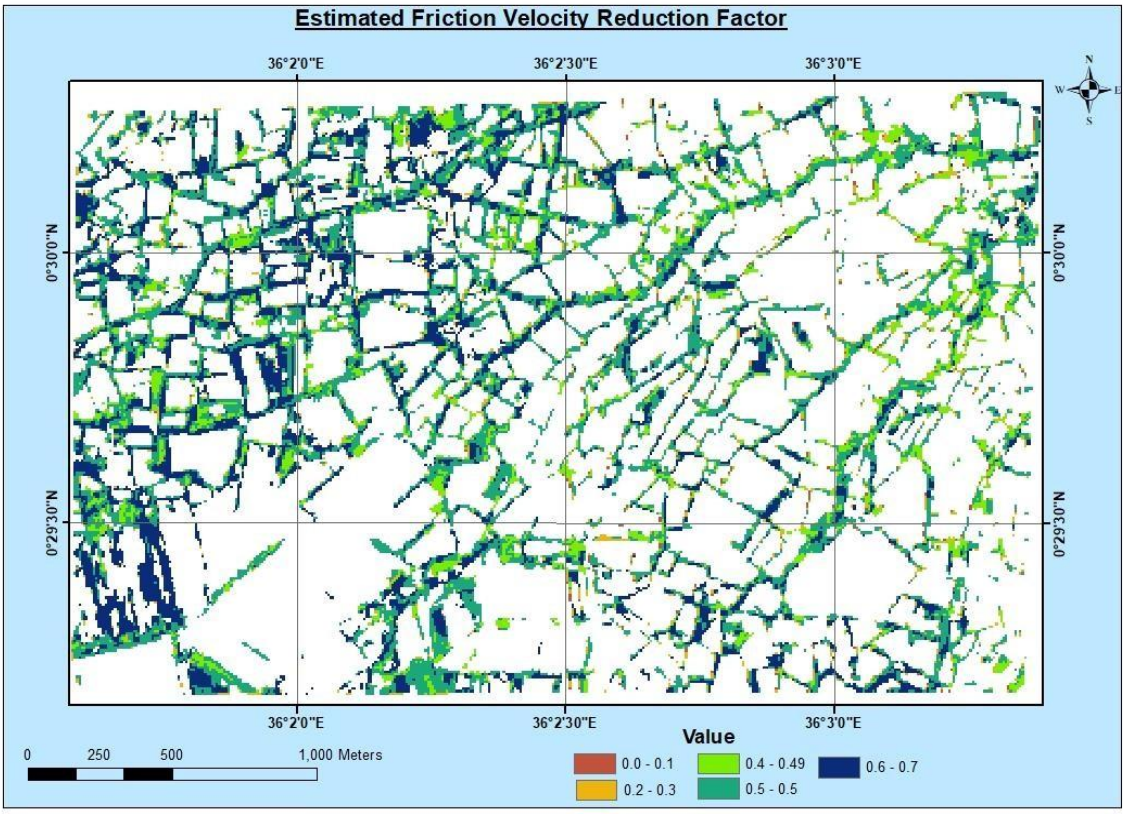

Figure 4.3: Estimated Friction Velocity Reduction Factor

4.1.3.2 Validation

The justification for the efficiency of windbreaks was further supported by a comparison between the moments before and after trees were grown. An examination of erosion values in farmlands for 2020; Figure 4.4(b) and 2010; Figure 4.4(a) revealed a significant agreement with the study's findings. Specifically, higher erosion rates were observed in 2010 compared to 2020, indicating a reduction in erosion over time and aligning with the anticipated effects of the windbreaks. The erosion was greatly reduced from a maximum of 1.9 to 0.8 kg/ha within the region.

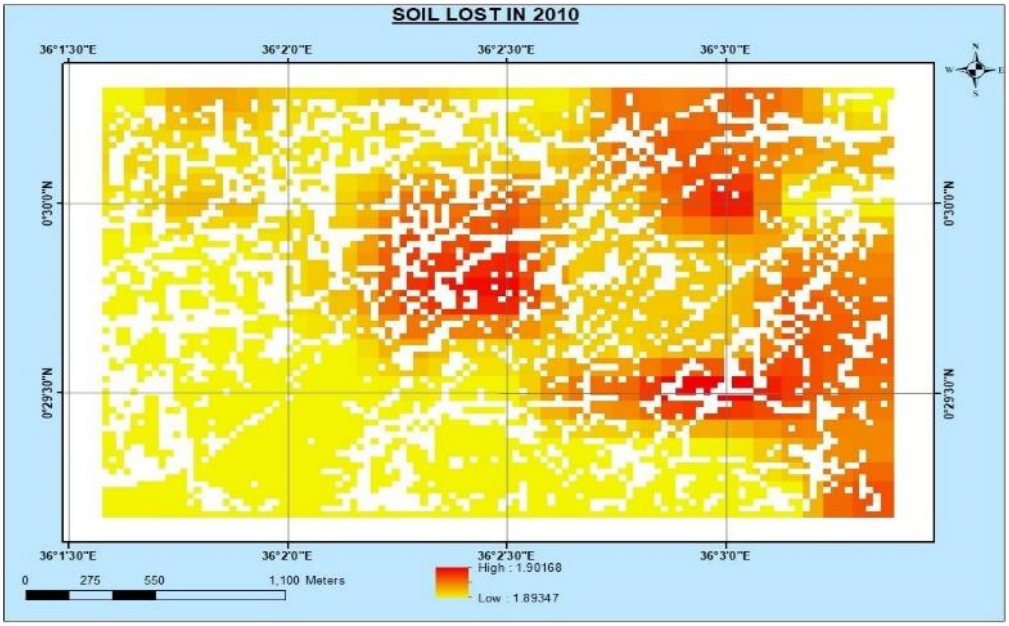

Figure 4.4(a): Soil lost in 2010

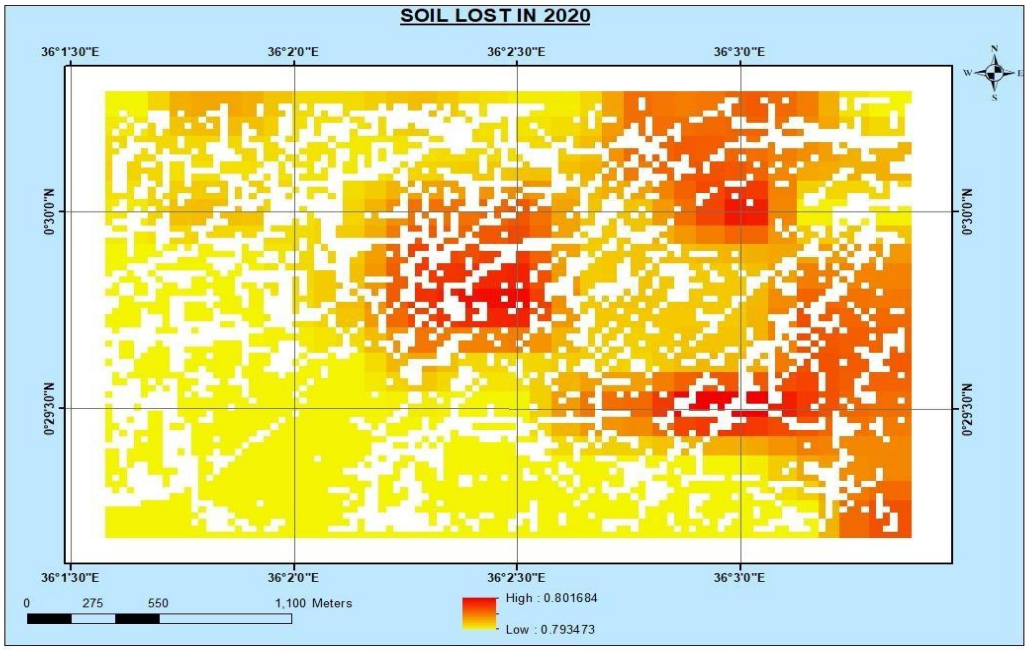

Figure 4.4(b): Soil lost in 2020

4.2 Discussion

4.2.1 Soil loss and susceptibility mapping

The climate erosivity in Baringo County exhibited a notable trend over the years, as evidenced by the results. In 1995, the erosivity factor was recorded at 0.14, which suggested a moderate erosive potential. This increased to 0.15 in 2000, indicating a slight rise. The year 2005 witnessed a further increment to 0.17, signifying a substantial increase in erosive forces. However, a decline is observed in subsequent years, with values dropping to 0.12 in 2010, 0.13 in 2015, and reaching the lowest at 0.05 in 2020. This reduction was a result of a mitigated erosive potential, influenced by changing meteorological conditions. The work by Boitt et al. (2020) on soil erosion and climate variability in the Kerio Valley Basin, Kenya, corroborates this fluctuating pattern, attributing changes to varying meteorological conditions over the years.

The erodibility fraction, a constant factor dependent on soil properties, remained relatively stable over the years. The values, ranging from 0.24 to 0.62, signified the soil's inherent susceptibility to erosion. The highest recorded value of 0.62 indicated a soil type more prone to erosion, while the lowest value of 0.24 indicated a soil with comparatively lower erosive potential. The soil crust factor, reliant on soil components also exhibited a notable constancy throughout the period from 1995 to 2020. With values ranging from 0.06 to 0.80, this factor reflected the stability of the soil surface against erosion. The higher values implied a more robust soil crust, indicating increased resistance to wind erosion. Conversely, the lower values suggested a less consolidated soil surface.

The surface roughness factor in Baringo, derived from land cover reclassification, exhibited noticeable trends. Initially, the landscape demonstrated heterogeneous roughness patterns, reflecting varied land cover characteristics. As the study progressed, a discernible trend emerges, with certain areas experiencing an increase in surface roughness, especially those which experienced natural vegetation growth or transitioning to more protective land covers.

Conversely, the areas with anthropogenic land use changes or reduced vegetation witness a decline in surface roughness. The surface roughness and soil erodibility fraction reflect inherent soil properties' role in erosion susceptibility, a conclusion also drawn by Chi et al. (2019) in their study on anthropogenic land use/cover changes and soil wind erosion in China.

Vegetation cover factor, derived from the Normalized Difference Vegetation Index (NDVI), was a pivotal factor in assessing the potential impact of wind erosion. The consistent decline in NDVI values from 1995 to 2020 signified an overall decrease in vegetation cover within Baringo County. In 1995, the NDVI was recorded at 0.96, indicating highest level of vegetation. Over subsequent years, there is a negative trend, with values reaching 0.66 in 2020. This findings are parallels to the study by Chi et al. (2022) on the effects of land use/cover change on soil wind erosion in the Yellow River Basin. The study found out that the downward trajectory resulted from a gradual decline in the extent and health of vegetation, thus implying a negative influence on wind erosion.

The temporal variation in maximum transport capacity for soil erosion, as depicted in the results, revealed an intriguing trend over the years. Notably, from 1995 to 2005, there was a substantial increase in maximum values, peaking at 4.71 in 2005, indicating heightened susceptibility to soil erosion during that period. The subsequent years, however, witness a slight decline in maximum transport capacity, reaching a value of 3.37 in 2020.The findings are similar to the study by Azimzadeh et al. (2022) on studying the field scale spatio-temporal variability of wind erosion transport capacity and soil loss at Urmia Lake. The study found out that an increase in maximum transport capacity resulted in an increase in wind erosion, which agrees with the finding of this study.

The escalating trend in critical field length, culminating in its peak in 2005, indicated a concerning amplification of the susceptibility of agricultural fields to wind-induced soil erosion. The rise in critical field length implied an expanding area affected by wind-driven soil erosion over the years. Contributing factors included changes in land use, variations in soil properties, and alterations in crop cover dynamics.

The upward trend in amount of soil lost indicated an intensification of wind erosion processes in the region. It suggested that over the years, factors contributing to soil vulnerability, have exacerbated the erosive potential of wind. The fluctuation in soil loss values from 2005 onwards is attributed to a complex interplay of factors. Changes in land use, particularly increased agricultural activities or urbanization, variations in climatic conditions, such as altered wind patterns or precipitation, which influence the erosive potential of the landscape.

The linear fuzzy membership function successfully transformed the datasets in the sensitivity mapping, to a standardized 0-1 scale, with 1 indicating the highest sensitivity and 0 implying no sensitivity. The maps, derived from the fuzzification process, revealed spatial patterns of erosion susceptibility for Climate Erosivity, Erodible Fraction, Crustal Erosivity, Surface Roughness, and Vegetation Cover.

High values in these maps pinpointed areas that were highly susceptible to wind-induced soil erosion during the study period, while low values represent regions with minimal sensitivity. These Sensitivity maps provided a visual and quantitative basis for identifying priority areas for targeted soil conservation efforts and land management strategies in Baringo County. The obtained results from the study aligns with research by Fenta et al., (2016) which focused on land susceptibility to erosion risks in East Africa. The results of susceptibility mapping and comparisons with Land Use/Land Cover (LULC) data agree with the findings obtained in the current study, highlighting the consistency in identifying vulnerable areas prone to erosion.

4.2.2 Analyzing the Impacts of land use/cover changes on soil wind erosion

The changes observed in Land use/cover classes areas presented a landscape transformation. The increase in bare land from 1995 to 2020 implied shifts in natural ecosystems, impacting soil stability and wind erosion resistance. Concurrently, the substantial expansion of Farmland by around 78000 ha signified the intensification of agricultural practices, potentially altering surface conditions and influencing wind erosion dynamics. The reduction of Forested areas by nearly 18000 ha implied significant deforestation or land-use changes, affecting biodiversity and potentially increasing wind erosion vulnerability.

Conversely, the considerable growth in Built-up areas by approximately 56200 ha indicated rapid urbanization, contributing to altered surface roughness and consequently influencing local wind erosion patterns. The reduction in forested areas and growth in built-up areas align with the global narrative of deforestation and urban expansion impacting soil stability and erosion susceptibility. Zhang et al. (2018) highlighted these impacts in Inner Mongolia, presenting a complementary perspective that reinforces the current study's observations.

The quantitative analysis of land susceptibility to wind erosion provides valuable insights into the varying degrees of vulnerability across different land cover classes. The results revealed notable disparities in susceptibility levels, with bare land exhibiting the highest vulnerability, followed by farmland, forested areas, and built-up areas. These findings show the impact of land use/cover on wind erosion susceptibility.

The high susceptibility of bare land to wind erosion, as evidenced by a significant portion falling in the low and moderate susceptibility categories, is attributed to the arid conditions and sparse vegetation cover prevalent in these areas. The lack of vegetation exposes the soil surface to erosive forces, making it more prone to erosion. However, the presence of a considerable percentage in the very low susceptibility category suggests that certain bare land areas possess natural features or soil properties that mitigate erosion risks to some extent.

Conversely, farmland displayed a more balanced distribution of susceptibility levels, with agricultural practices contributing to a more stabilized soil structure. The higher percentage in the low and moderate susceptibility categories reflects efforts to implement soil conservation measures and maintain vegetative cover, resulting in reduced vulnerability compared to natural landscapes. However, the presence of a notable percentage in the moderate susceptibility category highlighted the need for continued management practices to mitigate erosion risks associated with agricultural activities.

Forested areas demonstrated the lowest susceptibility to wind erosion, primarily due to the dense vegetation cover and complex structure of forests. The protective shield provided by the vegetation minimizes soil exposure to erosive forces, resulting in a higher percentage in the least susceptible categories. The minimal percentage of forested areas facing high susceptibility underscores the effectiveness of forests in erosion control and emphasizes their importance in preserving soil integrity and ecosystem resilience.

Built-up areas exhibit the lowest susceptibility to wind erosion, primarily due to the presence of impervious surfaces and structures that shield the soil from erosive forces. The high percentage in the very low susceptibility category reflects the protective nature of urban infrastructure, highlighting the role of built environments in reducing erosion risks. However, the presence of a small percentage in the moderate susceptibility category suggests the need for sustainable urban planning practices to address localized erosion concerns and maintain soil health in urban areas. The landscape transformation in Baringo County, characterized by an increase in bare land and expansion of farmland and built-up, resonates with the findings of Kogo et al. (2020), who observed similar trends and their impact on soil erosion in Western Kenya.

4.2.3 Evaluating the efficiency of windbreaks

The study, conducted in a roughly 288 Km^2 rectangular area within the Perkerra Irrigation Scheme. The absence of mountains or intricate forest ecosystems in the scheme simplified the study's scope. The key finding revealed an average width of approximately 4.8 meters for these shelterbelts. This measurement, derived through precise OBIA techniques, portrayed the consistent lateral spread of windbreaks, providing valuable insights into their spatial characteristics.

The assessment of optical porosity within the shelterbelt showcased a prevalent range of values spanning from 0.26 to 0.87. This critical metric served as an indicator of the extent to which wind can infiltrate or traverse the shelterbelt, providing valuable insights into its structural properties. Notably, higher values of optical porosity revealed an inverse relationship with the amount of wind passing through the shelterbelt.

The evaluation of vegetation efficiency against wind erosion, examination of average tree height revealed a range from 3 to 10.5 m in the region. The observed variability in tree heights within the landscape implied that, taller trees offered more effective resistance to wind forces. Conversely, shorter trees have a lesser impact. This analysis shows the importance of considering the vertical structure in assessing the overall efficiency of vegetation, particularly trees, in protecting the region against wind erosion. In the assessment of shelter belt efficiency against wind erosion, the Euclidean distances calculated revealed that shelter belts situated with smaller distances along this direction were more effective in mitigating wind erosion.

The computation of the friction velocity reduction factor enabled quantifying the effectiveness of windbreaks against wind erosion. The obtained values, ranging from 0.4 to 0.7, delineated a linear relationship between the friction velocity reduction factor and windbreak efficiency. Higher values indicated more effective windbreaks in reducing wind forces and minimizing wind erosion. This highlighted the importance of considering windbreak characteristics, such as width, porosity, height, and distance, in erosion control strategies.

Insights from studies such as the one by Yang et al. (2021) provide further support for the findings regarding the efficiency of windbreaks. This research, which evaluated wind protection by windbreaks using remote sensing and geographic information systems, concurs with the current study's identification of the friction velocity factor as a useful indicator for assessing windbreak efficiency. This agreement reinforces the utility and applicability of friction velocity as a static measure for evaluating the effectiveness of windbreaks in mitigating wind erosion.

4.3 Validation

A direct comparison of the wind erosion risk estimates with measured data was not feasible due to the absence of ground-based soil loss observations from wind erosion in Baringo county. Thus, to identify potential dust sources and assess the wind erosion risk map's credibility; Figure 4.1, a map depicting the mean annual dust storm frequency; Figure 4.8 was created using SeaWiFS Level-3 daily gridded data. An overlay analysis of Figures 4.1 and 4.8 allowed the production of a confusion matrix; Table 4.3 to evaluate the correspondence between the wind erosion index and the dust storm frequency.

This necessitated the use of SeaWiFS Level-3 daily Aerosol Optical Depth (AOD); Figure 4.7 and Angstrom Exponent (AE); Figure 4.6 data spanning from 2000 to 2010.This data served as a stand-in for atmospheric dust, with the frequency of dust storms calculated based on specific criteria; AOD > 0.25 and AE < 0.5. These values were chosen in line with the conditions set by Ginoux et al. (2010) to detect freshly emitted dust particles.

The long-term average frequency of dust storms was then determined and classified into five classes using the variance minimization classification scheme (Jenks and Caspall, 1971). Subsequently, an overlay analysis was conducted between the Index of Land Susceptibility to Wind Erosion (ILSWE) map and the mean annual frequency of dust storms, resulting in a confusion matrix; Table 4.3. This matrix allowed for a detailed evaluation of the agreement between the wind erosion index and the frequency of dust storms.

The assessment of accuracy revealed varying results for different wind erosion severity classes. The very slight wind erosion risk class demonstrated the highest evaluation accuracy at 89%, followed by the very high wind erosion risk class at 80%. Conversely, the moderate wind erosion class exhibited the lowest accuracy at 35%. Considering a correct classification as one where the ILSWE-based estimate of wind erosion risk matches the frequency of dust storms mapping result, the overall accuracy stood at 73%. This indicated a substantial agreement between the developed wind erosion index and the frequency of dust storms.

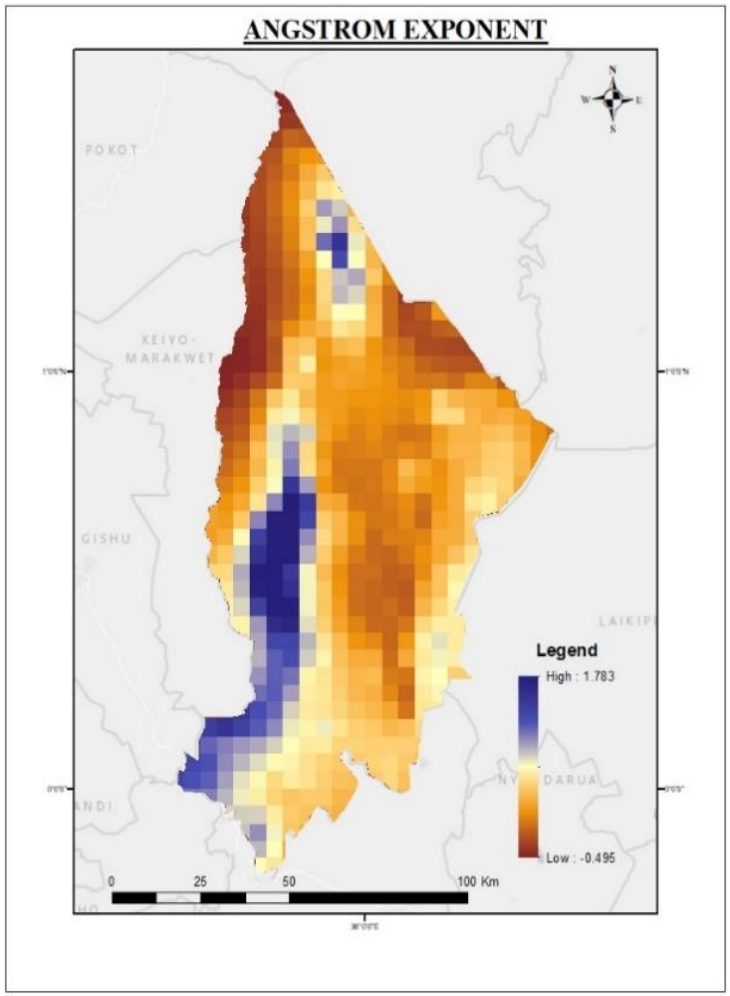

Figure 4.6: Angstrom Exponent

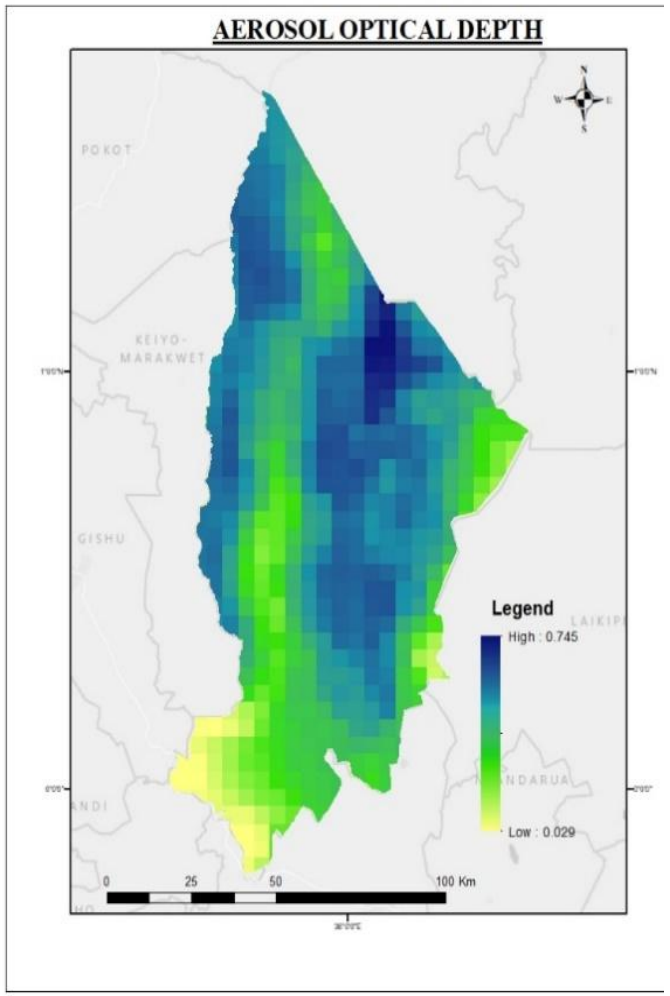

Figure 4.7: Aerosol Optical Depth

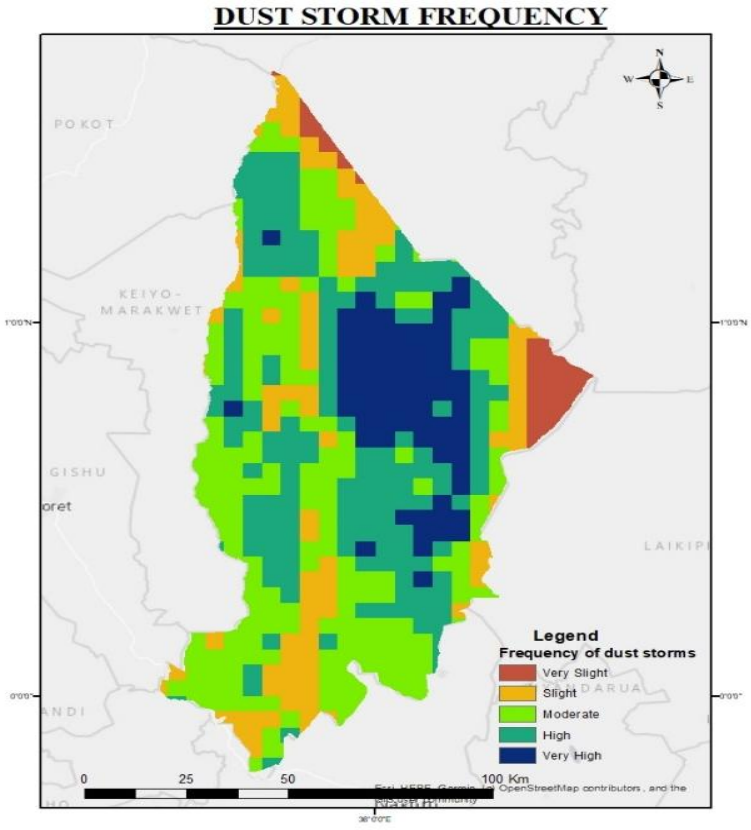

Figure 4.5: Dust Storm Frequency

Table 4.3: Error matrix comparing the agreement between wind erosion severity and mean annual frequency of dust storms

ILSWE	VERY SLIGHT	SLIGHT	MODERATE	HIGH	VERY HIGH
VERY SLIGHT	51.8	5	0.7	0.5	0.1
SLIGHT	7.7	6.6	0.7	0.7	0
MODERATE	1.7	3.2	1.6	1.9	0.2
HIGH	0.6	0.5	1.3	4.3	4.6
VERY HIGH	0.1	0.0	0.0	1.1	5.1
OVERALL ACCURACY	73%				

CHAPTER 5 CONCLUSION AND RECOMMENDATION

5.1 Conclusion

The RWEQ model analysis estimated wind erosion-induced soil loss in Baringo County from 1995 to 2020. Quantitatively, mean annual soil loss escalated from 27.89 in 1995 to 36.95 Kg/ha in 2020, signaling a 36% increase over the 25-year period. The peak soil loss was recorded at 37.72 Kg/ha in 2005. This trend points to an intensification of wind erosion processes over time in the study area.

The generation of an integrated susceptibility index map through overlay analysis of influencing factors enabled the delineation of regional erosion severity levels. In 1995, 78% of the county had very low to low susceptibility. By 2020, this decreased to 68%, while highly susceptible area doubled from 12% to 24%. This indicates an expanding footprint of wind erosion risk over the 25-year period.

Classification maps revealed that four main land cover classes underwent areal conversions that influenced wind erosion dynamics. Bare land area reduced by 24% from 123,712 in 1995 to 94,300 ha in 2020. Over the same period, Farmland area expanded notably by 78,000 ha, Built-up area rose exponentially by 56,200 ha, while Forest cover declined by nearly 18,000 ha. Overlay analysis uncovered that the conversion of Bareland to agricultural use escalated wind erosion risks.

Remote sensing-derived windbreak parameters were utilized to compute friction velocity reduction factors, serving as quantifiable indicators of erosion mitigation effectiveness. The range of obtained values, spanning between 0.4 and 0.7, suggests that thoughtfully designed windbreaks can appreciably reduce surface wind speeds, thus offering substantial protection from wind erosion across agricultural landscapes.

5.2 Recommendations

This study would have been improved if higher resolution images were used. Building on this, prioritizing the acquisition and utilization of high-resolution data to enable more precise wind erosion risk assessments. This will facilitate targeted conservation efforts at a finer, farm-specific level, contributing to more effective soil conservation strategies.

Utilizing updated data layers would have improved the study by giving real time information. Thus, consistently update data layers to ensure that erosion models accurately reflect the latest ground conditions. This practice enhances the reliability of long-term projections, providing stakeholders with timely and accurate information for informed decision-making.

Presence of ground observation sites would have improved validation of the project. Therefore, a need to implement a comprehensive approach by establishing long-term erosion monitoring stations across Baringo County. Supported by field experiments, these stations will play a pivotal role in validating and refining model estimates, ensuring their alignment with the local context and conditions.

A need for conducting more in-depth process-based research arose along the study in order to explore the impacts of soil moisture dynamics, vegetation impact, and the influence of extreme weather events on wind erosion. This detailed understanding will significantly enhance the predictive capabilities of erosion models, contributing to a more comprehensive and accurate assessment of wind erosion risks in the region.

REFERENCES

Aksoy, S., Akcay, H. G., & Wassenaar, T. (2010). Automatic Mapping of Linear Woody Vegetation Features in Agricultural Landscapes Using Very High Resolution Imagery. *IEEE Transactions on Geoscience and Remote Sensing*, *48*(1), 511–522. https://doi.org/10.1109/TGRS.2009.2027702

Bitog, J. P., Lee, I.-B., Hwang, H.-S., Shin, M.-H., Hong, S.-W., Seo, I.-H., Kwon, K.S., Mostafa, E., & Pang, Z. (2012). Numerical simulation study of a tree windbreak. *Biosystems Engineering*, *111*(1), 40–48. https://doi.org/10.1016/j.biosystemseng.2011.10.006

Boitt, M. K., Albright, O. M., & Kipkulei, H. K. (2020). Assessment of Soil Erosion and Climate Variability on Kerio Valley Basin, Kenya. *Journal of Geoscience and Environment Protection*, *8*(6), Article 6. https://doi.org/10.4236/gep.2020.86008

Borrelli, P., Lugato, E., Montanarella, L., & Panagos, P. (2017a). A New Assessment of Soil Loss Due to Wind Erosion in European Agricultural Soils Using a Quantitative Spatially Distributed Modelling Approach. *Land Degradation & Development*, *28*(1), 335–344. https://doi.org/10.1002/ldr.2588

Borrelli, P., Lugato, E., Montanarella, L., & Panagos, P. (2017b). A New Assessment of Soil Loss Due to Wind Erosion in European Agricultural Soils Using a Quantitative Spatially Distributed Modelling Approach. *Land Degradation & Development*, *28*(1), 335–344. https://doi.org/10.1002/ldr.2588

Brandle, J. R., Hodges, L., & Zhou, X. H. (2004). *Windbreaks in North American Agricultural Systems*.

Chi, W., Wang, Y., Lou, Y., Na, Y., & Luo, Q. (2022a). Effect of Land Use/Cover Change on Soil Wind Erosion in the Yellow River Basin since the 1990s. *Sustainability*, *14*(19), 12930. https://doi.org/10.3390/su141912930 Chi, W., Wang, Y., Lou, Y., Na, Y., & Luo, Q. (2022b). Effect of Land Use/Cover Change on Soil Wind Erosion in the Yellow River Basin since the 1990s. *Sustainability*, *14*(19), 12930. https://doi.org/10.3390/su141912930

Chi, W., Zhao, Y., Kuang, W., & He, H. (2019). Impacts of anthropogenic land use/cover changes on soil wind erosion in China. *Science of The Total Environment*, *668*, 204–215. https://doi.org/10.1016/j.scitotenv.2019.03.015

Chi, W., Zhao, Y., Kuang, W., Pan, T., Ba, T., Zhao, J., Jin, L., & Wang, S. (2021). Impact of Cropland Evolution on Soil Wind Erosion in Inner Mongolia of China. *Land*, *10*(6), Article 6. https://doi.org/10.3390/land10060583

Cleugh, H. A. (n.d.). *Effects of windbreaks on airflow, microclimates and crop yields*.

Cornelis, W. (2006). Hydroclimatology of wind erosion in arid and semiarid envirmonments. In *Dryland Ecohydrology* (pp. 141–159). https://doi.org/10.1007/1-4020-4260-4_9

Cornelis, W. M. (2006). HYDROCLIMATOLOGY OF WIND EROSION IN ARID AND SEMIARID ENVIRMONMENTS. In P. D'Odorico & A. Porporato (Eds.), *Dryland Ecohydrology* (pp. 141–159). Kluwer Academic Publishers. https://doi.org/10.1007/1-4020-4260-4_9

De Oro, L. A., Colazo, J. C., & Buschiazzo, D. E. (2016). RWEQ – Wind erosion predictions for variable soil roughness conditions. *Aeolian Research*, *20*, 139–146. https://doi.org/10.1016/j.aeolia.2016.01.001

Deng, R. X., Li, Y., Xu, X. L., Wang, W. J., & Wei., Y. C. (2017). Remote estimation of shelterbelt width from SPOT5 imagery. *Agroforestry Systems*, *91*(1), 161–172. https://doi.org/10.1007/s10457-016-9915-1

Deng, R., Xu, Z., Li, Y., Zhang, X., Li, C., & Zhang, L. (2022). Farmland Shelterbelt Age Mapping Using Landsat Time Series Images. *Remote Sensing*, *14*(6), 1457. https://doi.org/10.3390/rs14061457

E. L. Skidmore & J. Tatarko. (1990). STOCHASTIC WIND SIMULATION FOR EROSION MODELING. *Transactions of the ASAE*, *33*(6), 1893–1899. https://doi.org/10.13031/2013.31555

Efficiency evaluation of wind protection of windbreaks by remote sensing.pdf. (n.d.).

Ezenwa, L., Ibe, G., Ochor, N. O., & Ogbonna, O. (2018). Assessing the Impacts of Climate Variability on Livelihood Assets in Marigat and Mogotio Sub-County, Baringo County, Kenya. *Asian Journal of Geographical Research*, 1–14. https://doi.org/10.9734/ajgr/2018/v1i124670

Fenta, A. A., Tsunekawa, A., Haregeweyn, N., Poesen, J., Tsubo, M., Borrelli, P., Panagos, P., Vanmaercke, M., Broeckx, J., Yasuda, H., Kawai, T., & Kurosaki, Y. (2020). Land susceptibility to water and wind erosion risks in the East Africa region. *Science of The Total Environment*, *703*, 135016.

https://doi.org/10.1016/j.scitotenv.2019.135016

Fryrear, D. W., Sutherland, P. L., Davis, G., Hardee, G., & Dollar, M. (n.d.). *Wind Erosion Estimates with RWEQ and WEQ*.

Fryrear: Wind erosion estimates with RWEQ and WEQ - Google Scholar. (n.d.). Retrieved August 22, 2023, from https://scholar.google.com/scholar_lookup?title=Wind%20erosion%20estimates%20with%20RWEQ%20and%20WEQ%2C%20Proceedings%20of%20Conference%20Sustaining%20the%20Global%20Farm&author=D.%20Fryrear&publication_year=1999&pages=760-765

Ganasri, B. P., & Ramesh, H. (2016). Assessment of soil erosion by RUSLE model using remote sensing and GIS - A case study of Nethravathi Basin. *Geoscience Frontiers*, *7*(6), 953–961. https://doi.org/10.1016/j.gsf.2015.10.007

Gunawan, G., Sutjiningsih, D., Soeryantono, H., & W., S. (2013). Soil Erosion Estimation Based on GIS and Remote Sensing for Supporting Integrated Water Resources Conservation Management. *International Journal of Technology*, *4*(2), 147. https://doi.org/10.14716/ijtech.v4i2.110

Heisler, G. M., & Dewalle, D. R. (n.d.). *2. Effects of Windbreak Structure on Wind Flow*.

Jarrah, M., Mayel, S., Tatarko, J., Funk, R., & Kuka, K. (2020a). A review of wind erosion models: Data requirements, processes, and validity. *CATENA*, *187*, 104388. https://doi.org/10.1016/j.catena.2019.104388

Jarrah, M., Mayel, S., Tatarko, J., Funk, R., & Kuka, K. (2020b). A review of wind erosion models: Data requirements, processes, and validity. *CATENA*, *187*, 104388. https://doi.org/10.1016/j.catena.2019.104388

Kenney, W. A. (1987). A method for estimating windbreak porosity using digitized photographic silhouettes. *Agricultural and Forest Meteorology*, *39*(2–3), 91–94. https://doi.org/10.1016/0168-1923(87)90028-1

Kogo, B. K., Kumar, L., & Koech, R. (2020). Impact of Land Use/Cover Changes on Soil Erosion in Western Kenya. *Sustainability*, *12*(22), 9740. https://doi.org/10.3390/su12229740

Kučera, J., Podhrázská, J., Karásek, P., & Papaj, V. (2020). The Effect of Windbreak Parameters on the Wind Erosion Risk Assessment in Agricultural Landscape.

Journal of Ecological Engineering, *21*(2), 150–156. https://doi.org/10.12911/22998993/116323

Li, J., Ma, X., & Zhang, C. (2020). Predicting the spatiotemporal variation in soil wind erosion across Central Asia in response to climate change in the 21st century. *Science of The Total Environment*, *709*, 136060. https://doi.org/10.1016/j.scitotenv.2019.136060

Li, J., Okin, G. S., Tatarko, J., Webb, N. P., & Herrick, J. E. (2014). Consistency of wind erosion assessments across land use and land cover types: A critical analysis. *Aeolian Research*, *15*, 253–260. https://doi.org/10.1016/j.aeolia.2014.04.007

Liu, C., Zheng, Z., Cheng, H., & Zou, X. (2018a). Airflow around single and multiple plants. *Agricultural and Forest Meteorology*, *252*, 27–38. https://doi.org/10.1016/j.agrformet.2018.01.009

Liu, C., Zheng, Z., Cheng, H., & Zou, X. (2018b). Airflow around single and multiple plants. *Agricultural and Forest Meteorology*, *252*, 27–38. https://doi.org/10.1016/j.agrformet.2018.01.009

Liu, C., Zheng, Z., Cheng, H., & Zou, X. (2018c). Airflow around single and multiple plants. *Agricultural and Forest Meteorology*, *252*, 27–38. https://doi.org/10.1016/j.agrformet.2018.01.009

Mutanen, T., Sirro, L., & Rauste, Y. (2016). Tree height estimates in boreal forest using Gaussian process regression. *2016 IEEE International Geoscience and Remote Sensing Symposium (IGARSS)*, 1757–1760. https://doi.org/10.1109/IGARSS.2016.7729450

Ochieng, R., Recha, C., Bebe, B. O., & Ogendi, G. M. (2017). Rainfall Variability and Droughts in the Drylands of Baringo County, Kenya. *OALib*, *04*(08), 1–15. https://doi.org/10.4236/oalib.1103827

Řehácek, D., Khel, T., Kucera, J., Vopravil, J., & Petera, M. (2016). The character of windbreaks and their influence on mitigation of soil erosion. *Glasnik Sumarskog Fakulteta*, *114*, 219–226. https://doi.org/10.2298/GSF1614219R

Řeháček, D., Khel, T., Kučera, J., Vopravil, J., & Petera, M. (2017a). Effect of windbreaks on wind speed reduction and soil protection against wind erosion. *Soil and Water Research*, *12*(2), 128–135. https://doi.org/10.17221/45/2016-

SWR

Řeháček, D., Khel, T., Kučera, J., Vopravil, J., & Petera, M. (2017b). Effect of windbreaks on wind speed reduction and soil protection against wind erosion. *Soil and Water Research*, *12*(2), 128–135. https://doi.org/10.17221/45/2016-SWR

Santra, P., Moharana, P. C., Kumar, M., Soni, M. L., Pandey, C. B., Chaudhari, S. K., & Sikka, A. K. (2017a). Crop production and economic loss due to wind erosion in hot arid ecosystem of India. *Aeolian Research*, *28*, 71–82. https://doi.org/10.1016/j.aeolia.2017.07.009

Santra, P., Moharana, P. C., Kumar, M., Soni, M. L., Pandey, C. B., Chaudhari, S. K., & Sikka, A. K. (2017b). Crop production and economic loss due to wind erosion in hot arid ecosystem of India. *Aeolian Research*, *28*, 71–82. https://doi.org/10.1016/j.aeolia.2017.07.009

Scott, D. M., Mazurkiewicz, M., & Leeman, P. (1976). The long-term monitoring of ventilation rhythms of the polychaetous annelid Nereis virens sars. *Comparative Biochemistry and Physiology. A, Comparative Physiology*, *53*(1), 65–68. https://doi.org/10.1016/s0300-9629(76)80012-6

Vigiak, O., Sterk, G., Warren, A., & Hagen, L. J. (2003). Spatial modeling of wind speed around windbreaks. *CATENA*, *52*(3–4), 273–288. https://doi.org/10.1016/S0341-8162(03)00018-3

Visser, S. M., Sterk, G., & Karssenberg, D. (2005a). Wind erosion modelling in a Sahelian environment. *Environmental Modelling & Software*, *20*(1), 69–84. https://doi.org/10.1016/j.envsoft.2003.12.010

Visser, S. M., Sterk, G., & Karssenberg, D. (2005b). Wind erosion modelling in a Sahelian environment. *Environmental Modelling & Software*, *20*(1), 69–84. https://doi.org/10.1016/j.envsoft.2003.12.010

Wiseman, G., Kort, J., & Walker, D. (2009). Quantification of shelterbelt characteristics using high-resolution imagery. *Agriculture, Ecosystems & Environment*, *131*(1–2), 111–117. https://doi.org/10.1016/j.agee.2008.10.018

Wu, X., Fan, J., Sun, L., Zhang, H., Xu, Y., Yao, Y., Yan, X., Zhou, J., Jia, Y., & Chi, W. (2021). Wind erosion and its ecological effects on soil in the northern

piedmont of the Yinshan Mountains. *Ecological Indicators*, *128*, 107825. https://doi.org/10.1016/j.ecolind.2021.107825

Xie, Y., Tang, J., Gao, Y., Gu, Z., Liu, G., & Ren, X. (2023). Spatial distribution of soil erosion and its impacts on soil productivity in Songnen typical black soil region. *International Soil and Water Conservation Research*, *11*(4), 649–659. https://doi.org/10.1016/j.iswcr.2023.01.002

Yang, X., Li, F., Fan, W., Liu, G., & Yu, Y. (2021a). Evaluating the efficiency of wind protection by windbreaks based on remote sensing and geographic information systems. *Agroforestry Systems*, *95*(2), 353–365. https://doi.org/10.1007/s10457-021-00594-x

Yang, X., Li, F., Fan, W., Liu, G., & Yu, Y. (2021b). Evaluating the efficiency of wind protection by windbreaks based on remote sensing and geographic information systems. *Agroforestry Systems*, *95*(2), 353–365. https://doi.org/10.1007/s10457-021-00594-x

Yang, X., Yu, Y., & Fan, W. (2017). A method to estimate the structural parameters of windbreaks using remote sensing. *Agroforestry Systems*, *91*(1), 37–49. https://doi.org/10.1007/s10457-016-9904-4

Zhang, H., Fan, J., Cao, W., Harris, W., Li, Y., Chi, W., & Wang, S. (2018). Response of wind erosion dynamics to climate change and human activity in Inner Mongolia, China during 1990 to 2015. *Science of The Total Environment*, *639*, 1038–1050. https://doi.org/10.1016/j.scitotenv.2018.05.082

Zhang, H., Peng, J., Zhao, C., Xu, Z., Dong, J., & Gao, Y. (2021). Wind speed in spring dominated the decrease in wind erosion across the Horqin Sandy Land in northern China. *Ecological Indicators*, *127*, 107599. https://doi.org/10.1016/j.ecolind.2021.107599

Zhou, Z., Zhang, Z., Zhang, W., Luo, J., Zhang, K., Cao, Z., & Wang, Z. (2022). The Impact of Residences and Roads on Wind Erosion in a Temperate Grassland Ecosystem: A Spatially Oriented Perspective. *International Journal of Environmental Research and Public Health*, *20*(1), 198. https://doi.org/10.3390/ijerph20010198

Zhou, Z., Zhang, Z., Zhang, W., Luo, J., Zhang, K., Cao, Z., & Wang, Z. (2023). The Impact of Residences and Roads on Wind Erosion in a Temperate Grassland

Ecosystem: A Spatially Oriented Perspective. *International Journal of Environmental Research and Public Health*, *20*(1), Article 1. https://doi.org/10.3390/ijerph20010198

Zhou, Z., Zhang, Z., Zou, X., Zhang, K., & Zhang, W. (2020). Quantifying wind erosion at landscape scale in a temperate grassland: Nonignorable influence of topography. *Geomorphology*, *370*, 107401. https://doi.org/10.1016/j.geomorph.2020.107401

Zobeck, T. M., Parker, N. C., Haskell, S., & Guoding, K. (2000). Scaling up from field to region for wind erosion prediction using a field-scale wind erosion model and GIS. *Agriculture, Ecosystems & Environment*, *82*(1–3), 247–259. https://doi.org/10.1016/S0167-8809(00)00229-2